Hydrothermal plume dynamics on Europa: Implications for chaos formation

Jason C. Goodman,[1] Geoffrey C. Collins,[2] John Marshall,[3] and Raymond T. Pierrehumbert[4]

Received 26 February 2003; revised 19 December 2003; accepted 12 January 2004; published 20 March 2004.

[1] Hydrothermal plumes may be responsible for transmitting radiogenic or tidally generated heat from Europa's rocky interior through a liquid ocean to the base of its ice shell. This process has been implicated in the formation of chaos regions and lenticulae by melting or exciting convection in the ice layer. In contrast to earlier work, we argue that Europa's ocean should be treated as an unstratified fluid. We have adapted and expanded upon existing work describing buoyant plumes in a rotating, unstratified environment. We discuss the scaling laws governing the flow and geometry of plumes on Europa and perform a laboratory experiment to obtain scaling constants and to visualize plume behavior in a Europa-like parameter regime. We predict that hydrothermal plumes on Europa are of a lateral scale (at least 25–50 km) comparable to large chaos regions; they are too broad to be responsible for the formation of individual lenticulae. Plume heat fluxes (0.1–10 W/m^2) are too weak to allow complete melt-through of the ice layer. Current speeds in the plume (3–8 mm/s) are much slower than indicated by previous studies. The observed movement of ice blocks in the Conamara Chaos region is unlikely to be driven by such weak flow. *INDEX TERMS:* 6218 Planetology: Solar System Objects: Jovian satellites; 5418 Planetology: Solid Surface Planets: Heat flow; 5430 Planetology: Solid Surface Planets: Interiors (8147); 4540 Oceanography: Physical: Ice mechanics and air/sea/ice exchange processes; 4568 Oceanography: Physical: Turbulence, diffusion, and mixing processes; *KEYWORDS:* chaos, Europa, hydrothermal plumes

Citation: Goodman, J. C., G. C. Collins, J. Marshall, and R. T. Pierrehumbert (2004), Hydrothermal plume dynamics on Europa: Implications for chaos formation, *J. Geophys. Res.*, *109*, E03008, doi:10.1029/2003JE002073.

1. Introduction

[2] Observational evidence for the existence of a liquid water layer beneath Europa's icy surface is accumulating rapidly. Spacecraft gravitational studies indicate a low-density layer of water and/or ice between 80 and 170 km thick [*Anderson et al.*, 1998]. Magnetometer measurements [*Kivelson et al.*, 2000; *Zimmer and Khuruna*, 2000], require the presence of a layer of conductive material, most likely saline water, near the surface. A large number of geological features on Europa's surface, including the number and shape of craters and the orientation and patterns of planetary-scale cracks, can be explained by the presence of a liquid layer; see [*Pappalardo et al.*, 1999b; *Greenberg et al.*, 2002; *Greeley et al.*, 2003] for a review. Many of the geological observations are also consistent with a warm ductile ice layer, but taken together with the magnetic field data, a liquid ocean layer seems to be the most plausible explanation. For the purposes of this paper, we shall assume that a substantial liquid layer does, in fact, exist.

[3] In Europa's "chaos" regions (of which the Conamara region is the archetype), the original crust appears to have been broken into sharp-edged polygonal blocks; these "ice rafts" are surrounded by rough-textured, low-lying "matrix" material. The blocks are translated and rotated from their original orientations [*Spaun et al.*, 1998]. The scene is reminiscent of tabular Antarctic icebergs locked in a matrix of sea ice, but the true formation process remains one of the major outstanding questions in the study of Europa [*Greeley et al.*, 2003].

[4] Two classes of models have been proposed to explain the formation of chaos and other localized surface disruptions. The first [*Pappalardo et al.*, 1998; *Nimmo and Manga*, 2002] invokes solid-state convection within the ice shell. In this model, chaos regions form over upwelling ice diapirs; salts within the ice may allow some partial melting to occur [*Head and Pappalardo*, 1999; *Pappalardo et al.*, 1999a].

[5] The second [*Greenberg et al.*, 1999] suggests that chaos regions denote areas where, as a result of local heating of the ice base, "melting from below reaches the surface, so that a lake of liquid water is exposed"

[1]Department of Physical Oceanography, Woods Hole Institute of Oceanography, Woods Hole, Massachusetts, USA.
[2]Department of Physics and Astronomy, Wheaton College, Norton, Massachusetts, USA.
[3]Department of Earth, Atmospheric, and Planetary Sciences, Massachusetts Institute of Technology, Cambridge, Massachusetts, USA.
[4]Department of Geophysical Sciences, University of Chicago, Chicago, Illinois, USA.

0148-0227/04/2003JE002073

[*Greenberg et al.*, 2002]. Here, the matrix represents refrozen water or slush and the blocks are pieces of thicker crust that have broken off and drifted into the interior of the melted zone.

[6] In addition to large chaos provinces like Conamara, Europa also possesses vast numbers of smaller, subcircular bumps or depressions; many of these have lumpy textures similar to matrix material. Similarities between these features and large chaos regions has led many [*Greenberg et al.*, 1999; *Spaun et al.*, 2002; *Figueredo et al.*, 2002] to suggest that they are also formed by the same process which generates large chaos regions. The vast majority of these features, variously described as "lenticulae" [*Spaun et al.*, 2002] or "small chaos features" [*Riley et al.*, 2000], are smaller than 15 km across.

[7] Whatever formation mechanism is proposed, chaos is thought to represent the result of some thermal modification of the surface. Tidal forcing is generally accepted as the most likely source for the heat required to maintain the liquid layer [*Peale*, 1999; *Spohn and Schubert*, 2003], and to drive this modification. However, in the absence of detailed information about the rheology of Europa's rocky interior and ice layer, the magnitude of this heating is poorly constrained.

[8] The melt-through model for chaos formation requires that a large amount of heat to be concentrated into a small area at the base of the ice layer. This heat must be communicated from the rocky interior to the ice layer, through the intervening liquid water layer. The behavior of the water layer strongly affects this heat transport, and imposes its own space and timescales on the delivery. Thus understanding the fluid dynamics of the ocean layer can help us choose between chaos formation models.

[9] Several authors [*Greenberg et al.*, 1999; *Thomson and Delaney*, 2001; *Collins et al.*, 2000] consider the effect of warm, buoyant hydrothermal plumes, fed by geothermal energy at the base of Europa's liquid layer, which rise through the ocean layer to warm the base of the ice. This localized heat source might drive the localized disruption seen in chaos regions, by melting partially or completely through the ice layer, or by exciting solid-state convection within the ice itself. Are the physical parameters of hydrothermal plumes (dimensions, time scales, heat fluxes and velocities) consistent with what is known of the chaos regions, or must we seek another explanation for them?

[10] In this work, we describe hydrothermal plume dynamics on Europa, using theoretical ideas gained by the study of convection in Earth's ocean. We also show the results of several simple laboratory experiments designed to pin down unknown scaling constants, and to provide visual demonstrations of plume behavior under Europa-like conditions. The results of this analysis lead to new insight into the formation of chaos regions on Europa.

[11] The goals of this study are similar to those of [*Thomson and Delaney*, 2001], who also considered the behavior of hydrothermal plumes in a Europan ocean. However, our approach, results, and conclusions are quite different. Thomson and Delaney's pioneering work (T&D hereafter) will be discussed and compared with our results throughout this study. In section 2.2, we provide a brief synopsis of their results; in section 3.1, we explain why the assumptions made by T&D might not be appropriate for Europa's ocean; and in section 5, we discuss the differences between our results and theirs.

2. Previous Work

2.1. Convection in Earth's Oceans

[12] The dynamics of convection in Earth's oceans has been considered for two major phenomena: the ascent of buoyant hydrothermal plumes from a seafloor source [*Helfrich and Battisti*, 1991; *Speer and Marshall*, 1995], and the descent of dense surface water, cooled by the atmosphere during wintertime, into the depths [*Marshall and Schott*, 1999; *Jones and Marshall*, 1993; *Maxworthy and Narimousa*, 1994; *Klinger and Marshall*, 1995; *Visbeck et al.*, 1996; *Jones and Marshall*, 1997; *Whitehead et al.*, 1996]. The dynamics of ascending versus descending plumes are the same; the key difference between these two phenomena is the size of the buoyancy source. Hydrothermal plumes are generally treated as point sources, arising from a single vent or collection of sources of negligible lateral extent. In the wintertime deep convection problem, buoyancy loss occurs over a much wider area.

[13] In both cases, convective fluid mixes as it rises/falls, forming rotating masses of diluted buoyant fluid whose motion and geometry are controlled by Coriolis interactions. (Coriolis control of fluid motion does not require flow velocities "in the water-skiing range," as has been asserted in the context of ice-raft drift [*Greenberg et al.*, 1999]. Flow becomes more geostrophic (more strongly Coriolis-controlled) at slower velocities [*Gill*, 1982; *Pedlosky*, 1987].) The column of plume fluid eventually undergoes "baroclinic instability," ejecting swirling blobs of fluid laterally to maintain a steady-state mass balance in the convective zone. The width of these ejected eddies is set by the "Rossby radius of deformation," a scale determined by the ratio of buoyancy forces to the Coriolis effect.

[14] Earth's ocean is stratified: its density increases significantly with depth. In a stratified fluid, a warm hydrothermal plume rises, mixing with its surroundings, until it reaches a "neutral buoyancy level," at which its density equals that of the surroundings. At this point, the plume spreads laterally [*Thomson et al.*, 1992; *Speer and Marshall*, 1995], forming a mushroom or anvil-shaped plume.

[15] The plume spreads until it grows wider than the Rossby radius of deformation r_D; beyond this limiting radius, the baroclinic instability process causes it to break up into smaller eddies [*Speer and Marshall*, 1995; *Helfrich and Battisti*, 1991]. These eddies spin away from the plume source. Thus a steady-state plume can be maintained, whose characteristic radius is r_D, which maintains a balance between geothermal heat supply and export via eddy shedding.

[16] A few laboratory experiments and numerical simulations have also been done on convection in an unstratified ambient fluid [*Fernando et al.*, 1998; *Jones and Marshall*, 1993]. This situation is not generally observed in Earth's oceans, but we will demonstrate that it may be relevant to Europan ocean dynamics. The overall dynamics of this situation are similar, though now there can be no neutral buoyancy level, so plumes ascend/descend until they strike the top/bottom boundary. This has important consequences

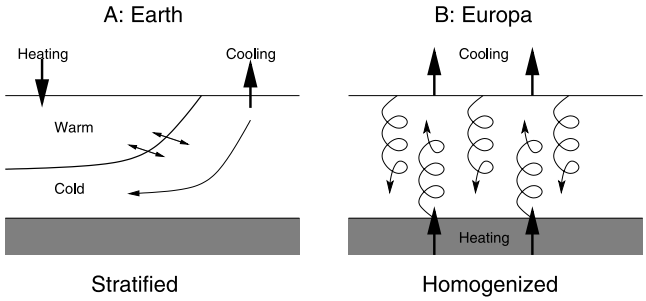

Figure 1. A: Lateral variation in surface heating/cooling allows cool water to slide beneath warm, causing Earth's oceans to become stratified. B: Heating at base, cooling at surface causes instability, turbulent mixing and homogenization of Europa's ocean.

for the geometry of the plumes and the scaling laws governing their behavior.

2.2. Hydrothermal Plumes on Europa

[17] Several authors [*Gaidos et al.*, 1999; *Chyba and Phillips*, 2002; *Schulze-Makuch and Irwin*, 2002] have discussed hydrothermal plumes on Europa as a possible energy source for life. The impact of hydrothermal plume heating on the morphology of the ice crust has been discussed informally for years, but only recently have quantitative descriptions appeared [*Collins et al.*, 2000; *Thomson and Delaney*, 2001]. *Collins et al.* [2000] considered the behavior of a warm plume ascending into an unstratified, nonrotating environment. They noted that since the warm plume tends to mix with its surroundings, its temperature upon reaching the ice/water interface is only a fraction of a millidegree above ambient, and suggested that such a tiny temperature difference would have little effect on the overlying ice.

[18] T&D provided the first detailed description of how heat can be communicated from hot spots on the surface of Europa's silicate interior, through a liquid layer, to the lower surface of the ice layer. They described how a hot patch of seafloor leads to a buoyant hydrothermal plume. The plume turbulently mixes with ambient fluid, but its width is constrained by Coriolis effects, and may rise to the ice/water interface. They used the existing literature on plumes in a rotating, stratified fluid (i.e., Earth's oceans) to compute the lateral extent and heat flux of the plume at the ice/water interface. They demonstrated that Coriolis effects ignored by *Collins et al.* [2000] play an dominant role in determining the structure and scales of the plume.

[19] For their choice of source intensity, T&D find plume widths of O(10 km) to O(100 km), in fair agreement with the scales of chaos regions as defined by [*Greenberg et al.*, 1999]. Their calculations suggest that the heat flux per unit area supplied by the plumes is sufficient to melt through the ice layer (assumed to be 2–5 km thick) in roughly 10^4 years. They note that, given a steady supply of heat, a hydrothermal plume periodically sheds warm baroclinic eddies into its surroundings, and speculate that the "satellite lenticulae" found near chaos regions may be formed as the warm eddies heat the overlying ice. Finally, they note that ice rafts in Conamara Chaos appear to have drifted in a clockwise direction during chaos formation [*Spaun et al.*, 1998]. They note that this is the expected direction of current flow at the top of a hydrothermal plume at the Chaos's location, and suggest that the blocks were transported by the current. After making an estimate of likely current speeds in the plume, they conclude that the currents could have pushed the blocks into their current orientation if open water existed in the Chaos region for about 22 hours.

[20] Thomson and Delaney's pioneering work brings an understanding of Earth's oceans to bear on the Europan chaos problem, and has inspired us to look more closely at the physical oceanography of Europan plumes, using different assumptions and more detailed analysis.

3. Hydrothermal Plume Dynamics: Theory and Scaling

[21] In this section, we attempt to find space, time, and velocity scales for a hypothetical hydrothermal plume within Europa's liquid layer. We derive these quantities using a scaling analysis, which provides an order-of-magnitude estimate, and includes an unknown constant factor of order unity. By fitting these scaling equations to data (both from published experiments and from our own simple experiments) we may find rough empirical values for the unknown factors.

3.1. Stratification

[22] The ascent of warm fluid from a seafloor source can be halted by either the stratification of the ambient fluid or the presence of a solid boundary. For terrestrial hydrothermal plumes, stratification is the principal impediment. The vertical density gradient also determines the Rossby radius r_D, and thus the width of the steady-state plume and the size of eddies shed by this plume (see section 2.1).

[23] When a solid boundary impedes the ascent [*Fernando et al.*, 1998; *Jones and Marshall*, 1993], the fluid is forced to spread out against the underside of the "ceiling" rather than at a neutrally buoyant level, and the plume fluid remains positively buoyant. Thus the presence of a barrier affects both the geometry and the buoyancy of the plume. For a neutrally buoyant plume, the dominant buoyancy contrast is the background vertical density gradient. In a boundary-impinging plume, the dominant contrast is between the ambient fluid and the plume fluid.

[24] Is Europa's liquid layer stratified? Earth's ocean (Figure 1a) is stratified because it is both heated and cooled at different locations along the upper surface. Water cooled at the poles slides beneath warm tropical water, forming stable stratification. If the dominant source of buoyancy in Europa's ocean is thermal rather than compositional, the situation is more reminiscent of a pot of water on a stove. Unlike a pot of water, Coriolis forces play an important role in the convective motion. The Coriolis-controlled convection in the Earth's liquid core is a closer analogue to Europa's ocean, except that in Europa's ocean, electromagnetic forces are unimportant. Note that Jupiter's magnetic field at Europa is 100 times smaller than Earth's intrinsic field [*Zimmer and Khuruna*, 2000], so that induction drag and field-line tension are utterly negligible [*Cowling*, 1957].

[25] Because of the basal heat input, Europa's ocean should be convectively unstable everywhere, and stable stratification should not occur. As basal heating attempts to place warm water under cold, the warm water rises, mixing turbulently with cold water sinking from above, erasing any vertical temperature gradient. In the inviscid, nonrotating limit, the stratification of a fluid heated from below is zero. Nonzero viscosity or rotation [*Julien et al.*, 1996] can lead to a slightly negative stratification (with dense water overlying light). Turbulence caused by the interaction of tidal currents with topography or by breaking internal gravity waves [*Hebert and Ruddick*, 2003] will also tend to eliminate stratification, assisting the basal heating (W. Moore, personal communication, 2003).

[26] Salinity variations caused by melting and freezing of Europa's ice might provide an additional buoyancy source at the upper surface of the liquid. This has the potential to produce stable stratification in some locations; we will consider the effect of this buoyancy source in section 7.

[27] Our argument assumes that Europa's liquid interior has a positive coefficient of thermal expansion: that is, that warm water is lighter than cold. This is true for most materials, including terrestrial seawater, but it is not true for fresh water (salinity < 25 g/kg) at low pressure (<30 MPa), near the freezing point. [*Melosh et al.*, 2002] describe the interesting and unusual dynamics of such an ocean, showing that it would undergo "paroxysmal overturn" events, leading to large-scale melting of the ice crust. Given our lack of knowledge of the ocean's composition, either our assumption or Melosh's could be true. For the present work, we will assume (as T&D do) that Europa's ocean is salty enough to ensure a positive coefficient of thermal expansion. We recognize that the results presented here are not valid if Europa's ocean satisfies Melosh's assumptions (and vice versa for Melosh's results).

[28] The key assumption of T&D's work is that Europa's ocean was "weakly stratified." The theoretical descriptions of plume dynamics they use [*Turner*, 1973; *Helfrich and Battisti*, 1991; *Lavelle*, 1999] assume that the ascending fluid can rise to a neutral buoyancy level. In contrast, T&D assumed that the plume encounters the ice/water interface (producing the chaos regions) before it becomes neutrally buoyant. These two assumptions are inconsistent and physically incompatible. The requirement that the plume reach the upper boundary implies that stratification is too weak to control the plume behavior. T&D's results break down if the stratification of Europa's oceans is zero or slightly negative, as we have argued above. Taken at face value, their equations would predict a maximum plume width which is zero, or takes an imaginary value.

[29] Thus, to understand Europan hydrothermal plumes, we must turn to the literature describing the ascent of buoyant plumes into an unstratified, homogeneous environment [*Fernando et al.*, 1998; *Jones and Marshall*, 1993]. In the rest of this section, we adapt the results of unstratified plume theory to Europa's oceans.

3.2. Working Assumptions

[30] In this analysis, we assume that Europa possesses a liquid water layer, and that this layer is unstratified. We assume, on the basis of comparison of gravitational data [*Anderson et al.*, 1998] with geomorphological studies [*Greeley et al.*, 2003], that the thickness H of the ocean layer is ~90 km. The conclusions derived below allow for a factor of 2 uncertainty in this value.

[31] We have no data on the heat output F from possible seafloor vent sites. For consistency with T&D's analysis, we assume that the heat flux is similar to that produced by large terrestrial mid-ocean-ridge hydrothermal systems: F = O(1–10 GW) [*Baker and Massoth*, 1987; *Thomson et al.*, 1992]. We will explore the parameter range between 0.1 and 100 GW, and demonstrate that the plume behavior is very weakly dependent on F.

[32] Below, we develop scaling equations for a buoyant hydrothermal plume arising from a point source. [*Fernando et al.*, 1998] demonstrate that plume behavior is independent of the diameter of the source, so long as it is smaller than the characteristic width of the plume (l_r, defined below). A similar set of equations have been derived for large, diffuse buoyancy sources [*Jones and Marshall*, 1993].

3.3. Scaling Analysis

[33] The derivation below follows the general scaling analysis technique used by many theoretical studies of convection [*Turner*, 1986; *List*, 1982; *Maxworthy and Narimousa*, 1994; *Jones and Marshall*, 1993; *Fernando et al.*, 1998; *Marshall and Schott*, 1999]. We rely particularly heavily on the work of *Fernando et al.* [1998] (henceforth FCA).

[34] While any effect of the hydrothermal plume on the overlying ice layer results from the steady-state action of the plume over many years, we gain a more natural understanding of the problem by considering the initial transient behavior of the plume. At time $t = 0$, we switch on a point-source of buoyancy, with buoyancy flux B:

$$B = g\Delta\rho/\rho_w\mu = b\mu \tag{1}$$

where ρ_w is the density of the unheated water, $\delta\rho$ is the density anomaly of the plume fluid, and μ is the volume flux, in units of m^3/s, of the plume. Lower-case b is the buoyancy anomaly of the plume fluid, in m/s^2; this is the acceleration which a parcel of plume fluid would experience in the absence of other forces. B is related to the heat flux F, and b to the temperature anomaly T':

$$B = \frac{g\alpha}{\rho_w C_{pw}} F \tag{2}$$

$$b = g\alpha T' \tag{3}$$

Here C_{pw}, and α are the heat capacity and thermal expansion coefficient of seawater, respectively. As the plume entrains ambient fluid, its volume flux μ increases while the buoyancy anomaly b declines. However, since B is proportional to the energy flux F, it is the same at every height in the plume.

3.3.1. Initial Behavior: Free Turbulent Convection

[35] In the first few moments after buoyant fluid leaves the source, Coriolis forces caused by planetary rotation are unimportant. Furthermore, the fluid is very far from the upper boundary, and so is unaffected by the finite depth H

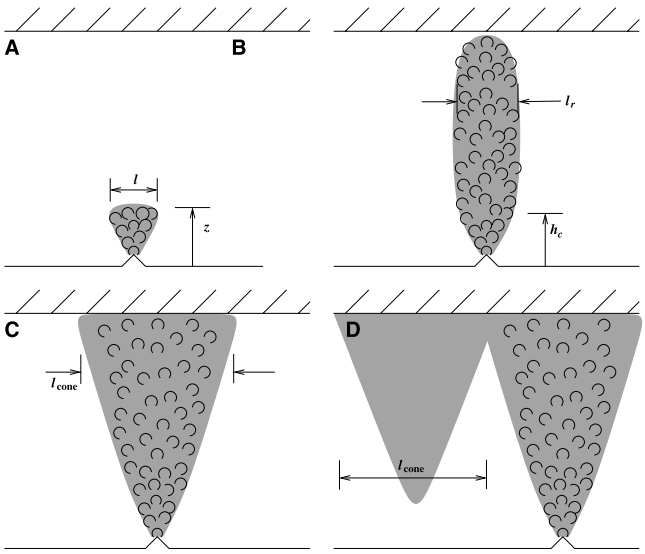

Figure 2. Stages in the evolution of a buoyant convecting plume. See text for full explanation. A: Free turbulent convection. B: rotationally controlled cylindrical plume. C: Baroclinic cone. D: Baroclinic instability.

of the ocean layer. Thus the buoyancy source B is the only relevant dimensional external parameter. (See Figure 2a.) We may form a length scale from B and the time t since the plume began:

$$L = \left(Bt^3\right)^{-1/4} \tag{4}$$

The plume's current height z above the source, and its width l, are both proportional to this characteristic lengthscale. Laboratory experiments [*Turner*, 1986] confirm that the plume grows upward and outward in a self-similar fashion, forming a conical plume.

[36] Let us investigate the physical mechanisms which lead to the scaling law (4). If no other forces act on it, the plume accelerates in response to the buoyancy b; the velocity w of the top surface of the plume is:

$$\frac{\partial w}{\partial t} = b \tag{5}$$

and thus the height z of the plume is:

$$\frac{\partial^2 z}{\partial t^2} = b \tag{6}$$

Now, using (1) and noting that the volume flux μ equals the cross-sectional area A of the plume head times its average vertical velocity w, we have:

$$B = Awb \tag{7}$$

If we assume a conical plume, with $z \sim L$ and $A \sim L^2$, (7) becomes (using (5) and (6)):

$$B \sim L^2 \frac{\partial L}{\partial t} \frac{\partial^2 L}{\partial t^2}$$

One may easily verify that (4) satisfies this differential equation, with boundary conditions $L = 0$ at $t = 0$, $w \to 0$ as $t \to \infty$.

[37] The volume flux μ must be a function of B and z, the only available parameters in the problem. The only dimensionally consistent choice for μ is:

$$\mu = k_\mu \left(Bz^5\right)^{1/3} \tag{8}$$

where k_μ is an empirically determined constant; $k_\mu \approx 0.15$, according to [*List*, 1982]. This expression may be confirmed by plugging (4) into the expression

$$\mu = Aw \sim L^2 \frac{\partial L}{\partial t}$$

[38] We may use (1) with (8) to find the buoyancy anomaly b:

$$b = B/\mu \sim \left(B^2 z^{-5}\right)^{1/3}$$

This relation for b may be used with (3) to find temperatures within the plume.

3.3.2. Influence of Rotation: Cylindrical Plumes

[39] Europa rotates about its axis once every 3.55 days, resulting in a Coriolis effect. The strength of the Coriolis "force" is controlled by the Coriolis parameter $f = 2\Omega \sin(\theta)$, where Ω is the angular rotation rate of the planet, and θ is the plume's latitude [*Gill*, 1982; *Pedlosky*, 1987]. Once the system has evolved for roughly one rotation period ($t \sim f^{-1}$), Coriolis forces become important; both f and B are now important external parameters in the problem. For Europan plumes in the energy flux range considered here, one may demonstrate that at $t \sim f^{-1}$, the plume's height is still much less than the ocean depth H. At this time, the characteristic length scale for the height and width of the plume (using (4)) is

$$l_{\text{rot}} \left(Bf^{-3}\right)^{1/4}$$

FCA find that, as the plume's height and width become larger than l_{rot}, the outward growth of the conical plume ceases. The plume begins to exhibit "Taylor column" [*Gill*, 1982; *Pedlosky*, 1987] behavior. Coriolis forces suppress vertical shear, and the flow changes from fully three-dimensional turbulence to quasi-two-dimensional, rotationally dominated motion. At height h_c, the plume ceases to expand in a cone shape, and begins to ascends as a cylinder of constant width l_r (see Figure 2b). From FCA's experimental data, we find:

$$h_c \approx 6\left(Bf^{-3}\right)^{1/4} \pm 20\%$$

$$l_r \approx 1.4\left(Bf^{-3}\right)^{1/4} \pm 15\%$$

Thomson and Delaney also describe the confinement of the plume by Coriolis effects. However, the confinement width described above depends on different parameters than those used by T&D.

[40] These rotationally constrained cylindrical plumes are essentially identical to those found in studies that use a finite-area source of buoyancy [*Jones and Marshall*, 1993; *Maxworthy and Narimousa*, 1994]. There, the dilution of plume water by entrainment ceases to change the plume's buoyancy and volume flux above the critical height h_c. We expect the same behavior here: above h_c, $\mu = \mu(z = h_c)$ and $b = b(z = h_c)$.

$$\begin{aligned} \mu_{\text{plume}} &\approx 0.15\left(Bh_c^5\right)^{1/3} = 3.5\left(B^3 f^{-5}\right)^{1/4} \\ b_{\text{plume}} &\approx 6.7\left(B^2 h_c^{-5}\right)^{1/3} = 0.30\left(Bf^5\right)^{1/4} \end{aligned} \tag{9}$$

3.3.3. Natural Rossby Number

[41] The cylindrical plume continues to rise until it encounters the upper boundary of the ocean. At this point, the total water depth H enters as a new external parameter, and it becomes possible to define a non-dimensional number from the external parameters B, f, and H:

$$h_c/H \sim Ro^* \equiv \left(Bf^{-3}\right)^{1/4}/H$$

Ro^*, the "natural Rossby number," measures the ratio of the height at which rotation becomes important to the total height of the fluid. If $Ro^* \ll 1$, the plume is controlled by planetary rotation for most of its ascent. If $Ro^* > 1$, the plume reaches the upper boundary before the effects of rotation are felt. We demonstrate in section 3.4 that $Ro^* \ll 1$ for hydrothermal plumes on Europa. As defined above, Ro^* is conceptually identical to the natural Rossby number defined for finite-area plumes by [*Marshall and Schott*, 1999] and [*Jones and Marshall*, 1993].

[42] The scaling laws described above can be recast in terms of Ro^*, H, and f:

$$\begin{aligned} h_c &\approx 6Ro^*H \\ l_r &\approx 1.4Ro^*H \\ \mu_{\text{plume}} &\approx 3.5(Ro^*)^3 H^3 f \\ b_{\text{plume}} &\approx 0.30Ro^*Hf^2 \end{aligned} \tag{10}$$

3.3.4. Interaction With the Upper Boundary: Baroclinic Cones

[43] When the rising plume encounters the upper surface, it must expand radially outward rather than upward. FCA's experiments show that the buoyant fluid spreads laterally over the entire depth, evolving from a cylinder to a straight-sided cone (see Figure 2c). Coriolis forces create an azimuthal "rim current" around the boundary of the plume.

[44] The onset of baroclinic instability (Figure 2d) limits the growth of this cone. FCA and others find that the plume becomes unstable when its width l_{cone} is of order r_D, the Rossby radius of deformation. At this point, it breaks up into multiple conical eddies.

[45] Different expressions for r_D are appropriate for different fluid density structures. Here, the ambient fluid is unstratified, and the density contrast is a relatively sharp jump between the warm, light water in the plume and the denser ambient fluid. Thus we should use the Rossby radius appropriate for a two-layer fluid [*Pedlosky*, 1987]:

$$r_D = \frac{\sqrt{b_{\text{plume}}H}}{f} \tag{11}$$

where b_{plume} is the buoyancy contrast between the plume and its surroundings.

[46] While the transition between plume- and non-plume fluid is not perfectly sharp, a 2-layer treatment is justified, since the density change is substantial, and narrow compared to the ocean depth. 2-layer approximations are quite successful in describing the circulation of Earth's upper ocean, whose density variations are even less sharp than our plumes' [*Pedlosky*, 1987].

[47] Recalling that $l_{\text{cone}} \sim r_D$, we combine (10) and (11) to obtain

$$l_{\text{cone}} = k_{lc}\sqrt{Ro^*}H \tag{12}$$

[48] It now remains to estimate k_{lc}. Unfortunately, FCA do not report an experimentally derived value for this constant. In section 4, we perform a series of simple tank experiments, and find a k_{lc} from them.

[49] We may also be interested in the time required for the formation of a baroclinic cone. This is equivalent to the time until baroclinic instability begins. The time to fill a cone is given by the volume of the cone divided by the volume flux into it:

$$\tau_{\text{bc}} = V/\mu = (\pi/12)l_{\text{cone}}^2 H/\mu = k_\tau (Ro^*)^{-2} f^{-1} \tag{13}$$

We must determine k_τ experimentally, as it is not reported by FCA.

[50] We are also interested in the characteristic current velocities of the plume system. The difference in azimuthal velocity between the top and bottom of the cone can be obtained using the thermal wind relation [*Gill*, 1982; *Pedlosky*, 1987]. For a two-layer fluid, this relation states

$$U_{\text{top}} - U_{\text{bottom}} = b/f\,\frac{\partial}{\partial r}h$$

where $\frac{\partial}{\partial r}$ is the slope of the interface separating the two layers, measured radially from the center of the plume. In our case,

$$\Delta U \sim \frac{2b_{\text{plume}}H}{fl_{\text{cone}}} \approx k_U\sqrt{Ro^*}Hf$$

[51] This is the difference in the velocities between the two layers. We must have information on pressure gradients near the surface to compute the actual velocities. T&D attempted to find an upper bound on this (see section 5), but no firm data are available. However, since we expect the fluid to be traveling in opposite directions in the two layers (because angular momentum is conserved as the fluid converges at the bottom and diverges near the top), ΔU is the maximum possible velocity in either layer; velocities half this are more likely.

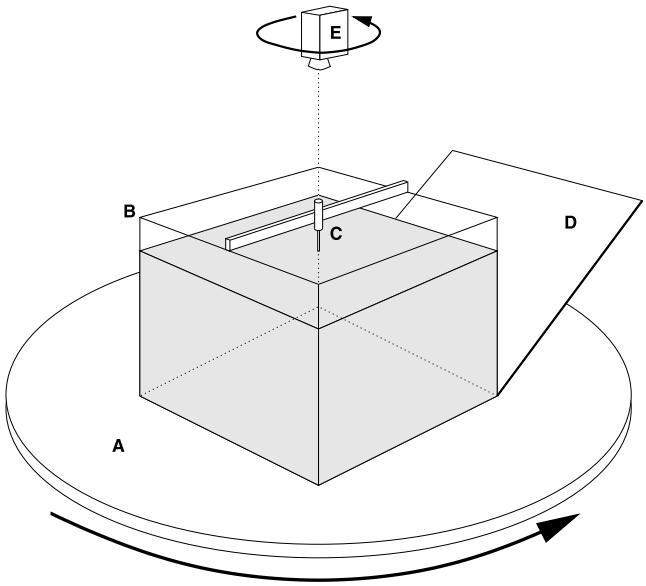

Figure 3. Illustration of experimental apparatus (not to scale). A: Rotating table. B: Lucite tank containing fresh water. C: Reservoir/nozzle apparatus containing dyed saline water. D: Angled mirror to present elevation view to camera. E: Co-rotating video camera.

[52] In FCA's experiments, the baroclinic eddies that form during baroclinic instability also have sizes comparable to l_{cone}. They are pushed around by currents generated by the convecting plume and by each other, and generally drift away from the source region. We expect that the speed at U_{drift} at which they move scales with ΔU.

$$\Delta U \sim U_{\text{drift}} \approx k_{\text{drift}} \sqrt{Ro^*} Hf \tag{14}$$

We determine k_{drift} experimentally in section 4.

[53] FCA find that the plume maintains its conical shape and diameter l_{cone} after the initial breakup. It reaches a steady-state balance, where the accumulation of buoyant fluid in the cone is balanced by the periodic ejection of baroclinic eddies.

3.4. Parameter Values for Europa

[54] All of the quantities derived above depend only on the Coriolis parameter f, the water depth H, and the hydrothermal buoyancy flux B. The Coriolis parameter $f = 2\Omega \sin\theta$ is simple to determine. The global average value of $|f|$ is $2\Omega/\pi = 1.3 \cdot 10^{-5}$ s^{-1} for Europa. At the latitude of Conamara Chaos (10°N), $f = 0.71 \cdot 10^{-5}$ s^{-1}.

[55] We shall assume that Europa's mean ocean depth is between 50 and 170 km. Gravitational measurements [*Anderson et al.*, 1998] suggest an ice + water layer between 80 and 170 km thick, so ocean depth must be less than 170 km. Investigating ocean depths less than 50 km would only be relevant for thin water layers with ice shells over 30 km thick.

[56] The buoyancy source B is related to the heat output F from a hydrothermal vent via (2). Lacking direct data for F, we shall consider values suggested by previous authors [*O'Brien et al.*, 2002; *Thomson and Delaney*, 2001], plus a substantial margin: we take $F = 0.1 - 100$ GW. The thermal expansion coefficient α in equation (2) depends on pressure, temperature, and salinity. For pressures corresponding to the base of a water + ice layer between 50 and 170 km thick, and salinities between 0 and 100 g/kg (Earth's oceans average 35 g/kg), $\alpha = 3 \cdot 10^{-4}$ K^{-1} ± 30%. This uncertainty is small compared to the range of F values we have chosen.

[57] Thus we predict values of B between 0.01 and 10 m^4/s^3. We can make robust estimates of plume behavior despite this wide range: note that the plume parameters derived in section 3.3 depend on B only through their dependence on the Ro^*, which is proportional to the fourth root of B. Therefore changing B by a factor of 1000 changes Ro^* by only a factor of 5.6. The most interesting parameters, the size and velocity scales of the baroclinic cone (l_{cone} and U), depend on $\sqrt{Ro^*}$, which varies by only a factor of 2.4 over a 1000-fold change in B. Using the parameters above, we expect hydrothermal plumes on Europa to lie within the regime $1/60 < Ro^* < 1/10$.

[58] This parameter regime is amenable to small-scale simulation in the laboratory. For example, a buoyancy source of 4 cm^4/s^3, released into a tank 30 cm deep, rotating at 1 rad/s, has a $Ro^* = 1/35$. Thus we can build a scale model of hydrothermal plumes in the laboratory. In the following section, we do so. The goal is to demonstrate the appearance and behavior of Europa-like plumes, to confirm the scaling parameters determined by FCA, and to find best-fit values for the undetermined constants k_{lc}, k_U, k_τ, k_{drift}.

4. Tank Experiment

4.1. Experimental Design

[59] The experimental apparatus (Figure 3) consists of a rotating table bearing a transparent cubical tank 50 cm on a side, containing water at ≈20°C. The rotation rate was varied between 0.25 and 1.5 rad/s; the water depth was varied between 20 and 40 cm. A reservoir containing dyed, salty water (salinity 25 ± 1 g/kg) is suspended over the tank. An injector, fed from the reservoir via a needle valve, permits about 0.23 ± 0.03 ml/s of salty water to enter the tank via an orifice 2 mm in diameter, located just beneath the surface.

[60] The denser injected fluid sinks, forming a convective plume. To compare the results of this experiment to that of a warm, rising plume, one should mentally flip the plumes upside down.

[61] The descending plume is visualized using a co-rotating video camera mounted above the tank. A mirror at a 45° angle is used to present an elevation view as well as a plan view to the camera.

[62] This apparatus has several weaknesses. First, the use of a narrow injector nozzle means that the fluid leaves the nozzle with a velocity of a few cm/s. The equations described above assumed a source of buoyancy with no initial momentum. However, scaling analysis [see *List*, 1982] suggests that the initial momentum becomes negligible <1 cm from the injector. FCA used a recirculatory apparatus to ensure a constant pressure at the injector. Our use of a simple small reservoir requires frequent re-filling during the experiment, causing variations in flow rate. FCA's use of a fluorescent dye illuminated by a sheet of laser light allows the imaging of a 2-d cross-section through the convecting fluid, while our technique allows us to image

Table 1. Parameter Values Used in Tank Experiments

Experiment	Vol. Flux, cm^3/s	Salinity	B, cm^4/s^3	H, cm	f, 1/s	*Ro**
1	0.25	25	4.64	30	1	1/20.4
2	0.25	25	4.64	30	1	1/20.4
3	0.23	25	4.27	30	2	1/35.1
4	0.23	25	4.27	30	2	1/35.1
5	0.23	25	4.27	30	0.5	1/12.4
6	0.23	25	4.27	37	3	1/59.0
7	0.23	25	4.27	20	2	1/23.4
8	0.23	25	4.27	20	1	1/13.9

only the silhouette of the entire 3-d plume structure, and introduces background clutter and reflections. Finally, our plan-view images are partly obscured by the support apparatus for the injector. Nevertheless, our technique allows us to illustrate and confirm the predictions of section 3.3.

[63] Table 1 shows the parameters used for the experiments. Since our analysis in section 3.3 predicts a lack of sensitivity to changes in B, we explored *Ro**-space by varying H and f.

4.2. Results

[64] Figure 4 shows the evolution of one experiment, which has a tank depth of 30 cm, rotating to give $f = 2\ s^{-1}$ (*Ro** = 1/35). The various structures predicted in section 3.3 are clearly visible. We see a conical freely convecting plume at t = 5 s in Figure 4a; a cylindrical rotationally controlled plume at t = 20 s in Figure 4b; the expansion of the cylindrical plume into a baroclinic cone at t = 60 s in Figure 4c; and the breakup of the cone into baroclinic eddies at t = 180 s in Figures 4d and 4e. After t = 180 s, the conical central plume remains, periodically shedding eddies to maintain a steady-state balance. The eddies gradually fill the tank.

[65] From this series of eight experiments, we measured the height h_c at which the plume changed from a conical to a cylindrical profile (see Figure 2b and equation (10)), the width of the descending cylindrical plume l_r, the time to baroclinic instability τ_{bc} (equation (13)), the width l_{cone} of the baroclinic cone at the onset of baroclinic instability (Figure 2c; equation (12)), and the drift velocity of the shed eddies U_{drift} (equation (14)). Error bars represent standard deviation of repeated measurements at different times and/or positions within the plume, as appropriate. No standardized criterion was used to define the somewhat diffuse edge of the plume fluid, though all the measurements were performed by one person to ensure consistency. Eddy drift velocities were found by measuring the change in position of eddy centers between two images taken 10–15 seconds apart. We were not able to measure the current velocities of the eddies and the plume, but as discussed in section 3.3.4, drift velocities and swirl velocities should be similar. This was corroborated by qualitative observation of

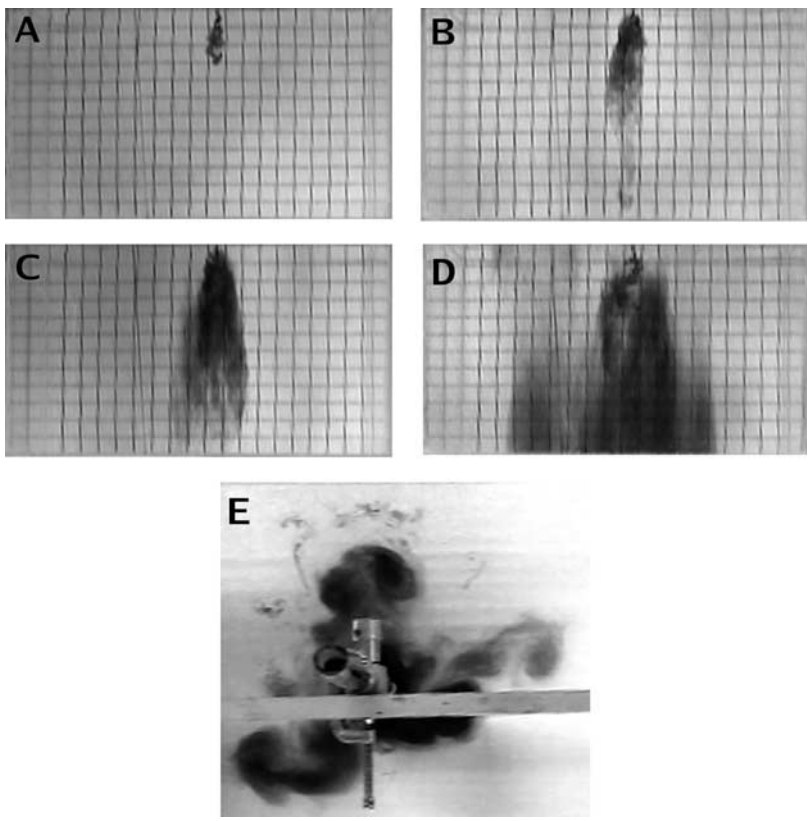

Figure 4. Evolution of a dense, sinking plume in a rotating tank; flip upside-down to compare with buoyant plume in Figure 2. For this experiment, B = 4.3 cm^4/s^3, H = 30 cm, $f = 2\ s^{-1}$. A: Conical free turbulent convection at t = 5 s. B: rotationally controlled cylindrical plume at t = 20 s. C: Baroclinic cone at t = 60 s. D: Eddy-shedding by baroclinic cone at t = 180 s (elevation). E: Plan view of eddy-shedding, t = 180 s. Grid-lines in elevation views are 2.5 cm apart. Flecks of dyed fluid at top of image (E) resulted from a small spill while refilling the injector reservoir.

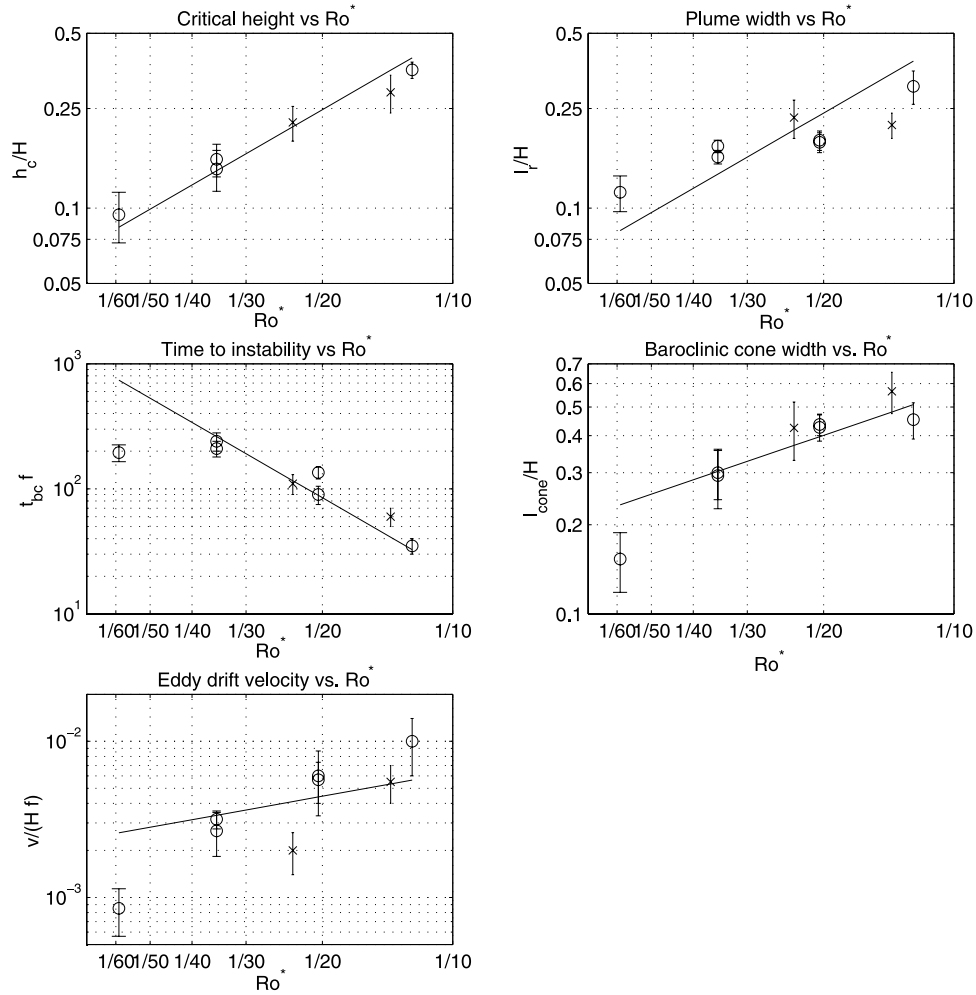

Figure 5. Comparison of experimental parameters with scaling laws. ×'s: experiments with $H = 20$ cm; ○'s: $H = 30$ or 37 cm. Solid lines show best-fit to scaling laws derived in section 3.3.

the movement of small-scale structures in the plumes and of markers scattered on the surface of the water.

[66] We compared the scaling laws derived in section 3.3 to these measurements, and found the best-fit constants of proportionality k. Figure 5 plots the best-fit scaling laws against the measured data; the best-fit k's are listed in Table 2.

[67] We find that the critical height follows the expected Ro^* scaling law very closely. Our best-fit value for k_h is compatible with the results of FCA. The width of the cylindrical plume l_r fits the data less perfectly, but is still within 25% of the observations. Our experimental data suggest that our cylindrical plumes are wider than those found by FCA: this difference may result from differences in measurement techniques or criteria, or unintended turbulence in our tank.

[68] Note that a scaling law proportional to $\sqrt{Ro^*}$ would fit our l_r data more accurately; given the limitations of our experiment, either experimental inaccuracy or a problem with the derived scaling law could be the cause of this misfit. We discuss this in more detail at the end of this section.

[69] The time to baroclinic instability quite closely follows a $(Ro^*)^{-2}$ scaling law, with the exception of the experiment at $Ro^* = 1/60$. This experiment demonstrated unusual behavior, described below. Baroclinic cone width is very close to the $\sqrt{Ro^*}$ scaling, except for the $Ro^* = 1/60$ experiment. Eddy drift velocity is not far from $\sqrt{Ro^*}$ behavior, again except for the $Ro^* = 1/60$ outlier; however, a scaling law proportional to Ro^* would fit the data more closely.

[70] The experiment performed near $Ro^* = 1/60$ behaved differently than the others. In this case, the plume never reached the bottom of the tank; instead, it appeared to break up into eddies before striking the bottom. The descending plume was extremely narrow ($l_r \approx 4$ cm across) with most turbulent activity at even smaller scales. At such small scales, molecular diffusivity and viscosity may become important. These would spread out momentum and buoyancy, increasing the effective width l_r of the plume. A

Table 2. Scaling Laws and Best-Fit Constant Values for Tank Experiments[a]

Quantity	Scaling Law	Best-Fit Constant	Best-Fit (FCA)
Critical Height	$h_c \approx k_h Ro^* H$	4.95	6
Cyl. Plume Width	$l_r \approx k_{lr} Ro^* H$	4.8	1.4
Time to Instability	$\tau_{bc} \approx k_\tau (Ro^*)^{-2} f^{-1}$	0.21	
Cone Width	$l_{cone} \approx k_{lc} \sqrt{Ro^* H}$	1.79	
Drift Velocity	$U_{drift} \approx k_{drift} \sqrt{Ro^* H f}$	0.020	

[a]Constant values found by FCA are also reported, where available.

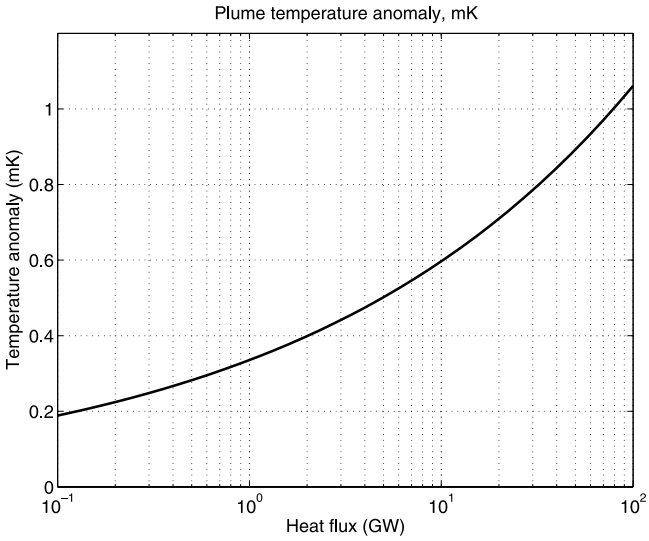

Figure 6. Predicted temperature anomaly of plume fluid, in milliKelvin. Plume output power $F = 0.1 - 100$ GW, coriolis parameter $f = 1.3 \cdot 10^{-5}$ s^{-1}.

broader plume would have a smaller buoyancy anomaly, and thus a smaller Rossby radius of deformation. This would reduce the cone width l_{cone} and the time to baroclinic instability τ_{bc}. All these effects match the observed deviation of this experiment from theoretical predictions.

[71] The theoretical scaling laws differ in some cases from the observations. This deviation is most significant ($\geq 3\sigma$) for the cylindrical plume width l_r; the best-fit scaling law is close to $l_r \sim \sqrt{Ro^*}$. Note that such a scaling law is inconsistent with FCA's results. Taken at face value, such a scaling would imply that the descending plume feels the influence of the tank bottom long before it comes into contact with it. Suppose for the moment that our theory is in error, and l_r really does vary as $\sqrt{Ro^*}$. In that case, repeating the analysis in sections 3.3.2–3.3.4 with this assumption leads to new semi-empirical predictions for baroclinic cone diameter, time to instability, and plume diameter. Such an analysis would predict $l_{cone} \sim Ro^* H$; $\tau_{bc} \sim f^{-1}$ (independent of Ro^*); and $v_{drift} \sim Ro^* Hf$. This alternate v_{drift} law is an improvement over the theoretical prediction; the l_{cone} law is slightly worse; and the alternate τ_{bc} is definitely wrong. Thus the theoretical prediction of section 3.3 does a better job in producing a physically consistent match to the sparse, noisy data.

[72] We intend to perform further experiments to identify the sources of the model/data mismatches, and more rigorously test the scaling laws presented in section 3.3. On the whole, though, we find acceptable agreement between theory and the present experiment, and we may now use these scaling laws to describe hydrothermal plumes on Europa, keeping in mind the limitations of the experiments.

4.3. Predicted Scales for Europan Plumes

4.3.1. Thermal Anomaly

[73] We may roughly estimate the temperature of the plume fluid impinging on the base of the ice layer, using (3) and (9).

[74] Figure 6 shows the value T', over the range of plume output power F described in section 3.4. Despite the wide variation in F of three orders of magnitude, predicted temperature anomalies vary by only a factor of 5. The predicted thermal anomalies are 0.2–1 milliKelvin. This range is much greater the estimate of 0.01 mK estimated by *Collins et al.* [2000], which neglected Coriolis effects; it is much smaller than T&D's estimate of 100 mK. We discuss the reason for this difference in section 5.3.

[75] While remarkably small, this temperature anomaly still represents a substantial amount of heat, which must either melt the ice or be conducted through it. And as we shall see, the temperature anomaly is enough to drive measurable currents in and around the plume.

4.3.2. Horizontal Scale

[76] Figure 7 uses (12) to predict l_{cone}, over the range of H and F described in section 3.4. Once again, the parameter is rather insensitive to the wide range of possible values of F. Predicted plume width varies by roughly a factor of 2 over the entire parameter range, between 25 and 50 km.

4.3.3. Heat Flux

[77] We now estimate the heat flux per unit area (in W/m^2) supplied to the ice by the plume. Referring to Figure 4e, we note that the eddies shed by the central plume remain in the vicinity for quite some time. The continual formation and ejection of new warm-core eddies supplies a significant amount of warm water out to several times l_{cone}. The warm eddies dissipate as they transfer heat to the base of the ice layer. Without information on the relative efficiency of lateral eddy heat transfer versus vertical conductive transfer, we cannot predict the precise area over which the heat is be delivered. However, the diameter D of the heating is probably somewhat larger than l_{cone}; that is, $D \approx pl_{cone}$, where $p \gtrsim 1$. Dividing the heat flux by the area of a disk of diameter D gives a rough estimate of heat flux per unit area.

[78] Figure 8 shows estimates of heat flux per unit area over our chosen range of H and F. For this figure, we have chosen $p = 2$. Uncertainty in p leads to a factor-of-several uncertainty in these flux estimates. As we vary heat output over three orders of magnitude, the area over which the heat

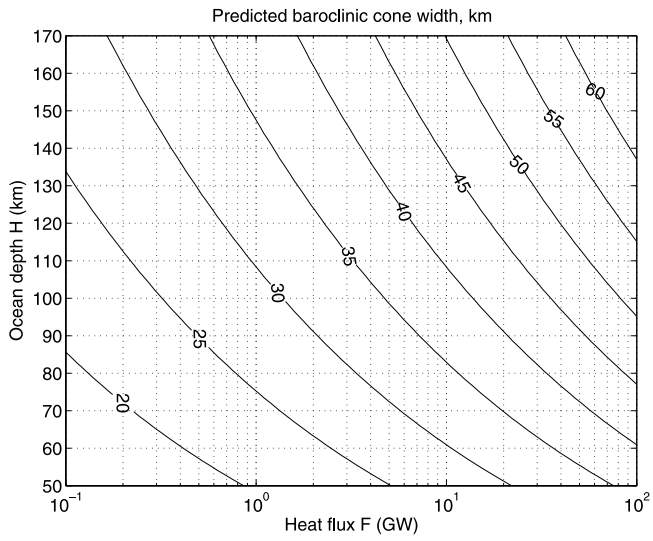

Figure 7. Predicted baroclinic cone width l_{cone}, in km, for hydrothermal plume fluxes $F = 0.1 - 100$ GW, and ocean depths $H = 50 - 170$ km. $f = 1.3 \cdot 10^{-5}$ s^{-1}.

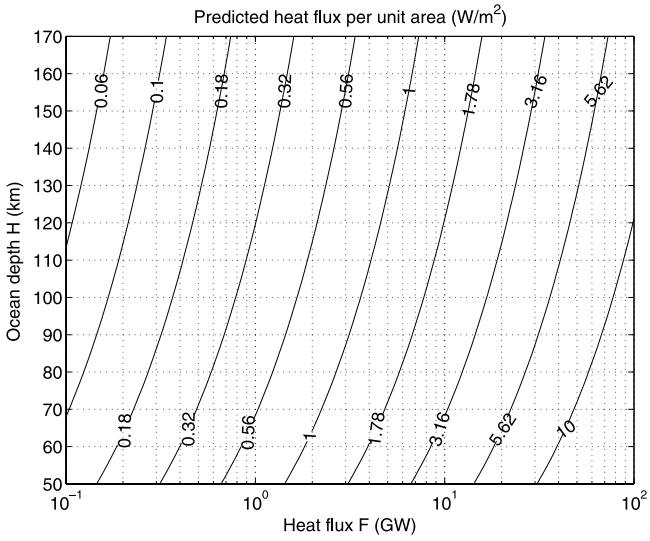

Figure 8. Predicted heat flux (W/m^2) delivered by a plume at the base of the ice layer over a range of plume output power $F = 0.1 - 100$ GW, and ocean depths $H = 50 - 170$ km. $f = 1.3 \cdot 10^{-5}$ s^{-1}, $p = 2$.

is supplied increases by only a factor of 5, resulting in a rather wide range of heat fluxes.

4.3.4. Velocities

[79] Figure 9 shows the predicted eddy drift rates, which range from 3 to 8 mm/s. As we remarked earlier, typical current speeds in the plume region should be similar to these values. Predicted velocities are much slower than the 0.1 m/s estimated by T&D. We discuss the reason for this, and its implications, in sections 5.4 and 6.4.

5. Comparison With *Thomson and Delaney* [2001]

[80] The basic assumptions used in this paper, our techniques, and our results differ significantly from the pioneering work of T&D. In this section, we discuss the differences between their description of plume behavior and ours. These differences also lead to disparate conclusions regarding the response of the ice layer to plume heating; these will be presented in section 6.

5.1. Stratification and Dynamical Regime of Plumes

[81] As discussed in section 3.1, we assume that the plume is governed by the dynamics of convection into an unstratified ambient fluid. In contrast, T&D assumed that Europa's oceans were "weakly stratified," by which they meant that the behavior was governed by the dynamics of convection in a stratified fluid, yet the stratification did not prevent the plume from rising through the entire depth of the ocean.

[82] We noted that T&D's assumption is self-contradictory; if stratification is too weak to halt the ascent of plume fluid to the top of the water layer, then it is inconsistent to assume that the ambient stratification orchestrates the dynamics. The density contrast between plume and ambient fluid is greater than the ambient stratification, a situation more consistent with the unstratified dynamics we use here.

[83] We also justify our assumption of zero stratification by noting that Europa's ocean is heated from below. In such cases, turbulent mixing erases the density gradient utterly.

[84] T&D's assumption of weak stratification allows them to put an upper bound on the strength of stratification within the ocean; stratification greater than this limit would prevent the plumes from reaching the ice. However, they cannot compute a lower bound. Thus their calculations of plume diameter, thermal anomaly, and heat flux, which depend on the stratification, also only provide upper/lower bounds, though this is not always obvious in their discussion.

5.2. Plume Shape and Evolution

[85] Both our study and T&D's describe a critical height at which the ascending plume fluid's motion becomes dominated by Coriolis effects. Both demonstrate that rotation restricts the radial expansion of the plume. Both agree that, once the plume strikes the base of the ice layer, it must spread laterally despite Coriolis influences. We concur that the Rossby radius of deformation r_D sets the maximum diameter of the plume; as it grows larger than r_D, it breaks up into baroclinic eddies.

[86] While qualitatively similar, the descriptions differ in detail. In describing the lateral spread of the plume, T&D portray a shallow lens of fluid spreading within the uppermost portion of the ocean (see their Figure 3b), with the bulk of the plume remaining narrow and cylindrical. Their diagram portrays the plume forming a "trumpet bell" shape. In contrast, our tank experiments and those of FCA demonstrate that the plume spreads at all depths, swelling to form an inverted cone.

[87] While we agree that the Rossby radius of deformation controls the final width of this cone, our expressions for this radius differ due to our differing assumptions. T&D use an expression valid for a stratified fluid (their equation (7)), which depends on the ambient stratification, ocean depth, and rotation rate, but not on the strength of the buoyancy source. Our expression is correct for a "two-layer" fluid; it depends on the buoyancy contrast between the plume and its surroundings, and thus on the strength of the source, but not on the ambient stratification.

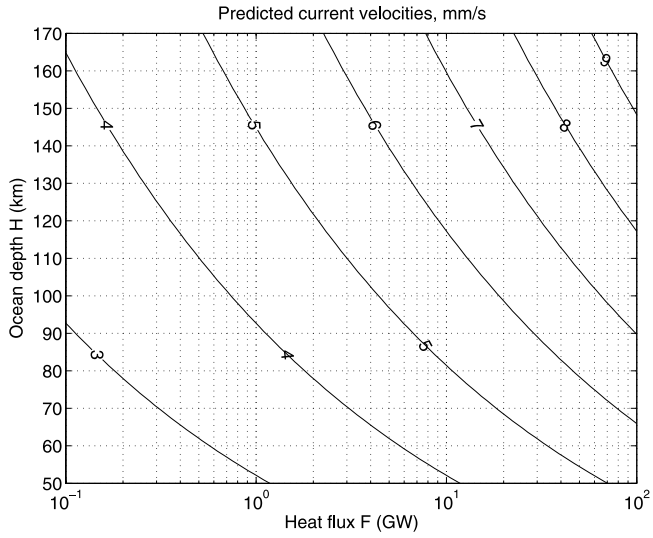

Figure 9. Predicted eddy drift velocities U_{drift}, in mm/s, for hydrothermal plume fluxes $F = 0.1 - 100$ GW, and ocean depths $H = 50 - 170$ km. $f = 1.3 \cdot 10^{-5}$ s^{-1}.

[88] If the ambient stratification is zero, as we have argued, then T&D's expression predicts a maximum plume width equal to zero, a physically unrealistic result. Thus a different dynamical balance than that assumed by T&D must take over in the limit of weak stratification.

[89] If one takes T&D's approach, and additionally assumes that the plume reaches a neutral buoyancy level in their stratified fluid at the precise moment that it comes in contact with the base of the ice, then the plume width would be equal to the upper-bound value they calculated, and would also roughly equal our prediction. However, there is no reason to expect that this special case actually occurs.

5.3. Thermal Anomalies Under the Ice

[90] T&D present a calculation of the thermal anomaly of the plume fluid that impinges on the base of the ice. Their equation (12) describes the temperature change in a fixed cylindrical volume of fluid heated by the hydrothermal source:

$$\Delta T = \frac{1}{\rho_w C_{pw} \pi r_D^2 d_\tau} \int_\tau F dt$$

where F is the heat source amplitude, τ is the time since the heat source was switched on, ρ_w and C_{pw} are the density and heat capacity of water, r_D is the radius of the cylindrical volume (equal to the Rossby radius of deformation), and d_τ is the thickness of the cylinder. To derive this equation from the definition of heat capacity, one must assume that r_D and d_τ are constant in time. They compute d_τ by supposing that the cylinder is gradually filled by accumulating plume water, so that its thickness at any time is:

$$d_\tau = \left(\frac{r_0}{r_D}\right)^2 \int_\tau w_0 dt$$

where r_0 and w_0 are the radius of the fluid source and the vertical velocity of the fluid it emits.

[91] Note the inconsistency in these equations: the first assumes that the plume's heat increases the temperature of a fixed volume of fluid. The second assumes that the plume's heat increases the volume of fluid at constant temperature. These assumptions cannot simultaneously be true. Taken together, the above equations would imply that in a bathtub filling with warm water, the steady flow of heat from the faucet would eventually cause the water in the tub to boil!

[92] The equation for d_τ is, in any case, incorrect: it assumes that the volume flux at the top of the plume is equal to the volume emitted by the sources at the bottom. Since the warm plume fluid mixes with and turbulently entrains ambient fluid as it rises, the volume flux at the top is many times the flux at the bottom [*Turner*, 1986].

[93] Our estimate of the temperature of the plume fluid at the ice/water interface emerges from the scaling laws for the final buoyancy of the plume fluid, which is set by turbulent mixing with the less buoyant ambient fluid. Since Coriolis effects act to inhibit this mixing, our estimate is 1–2 orders of magnitude greater than that of *Collins et al.* [2000]. It is 2–3 orders of magnitude less than T&D's.

5.4. Surface Current Velocity

[94] T&D attempt to estimate the speed of the plume's azimuthal rim current. By balancing centripetal and coriolis accelerations against pressure gradients caused by a sloping ocean free surface, they compute a maximum possible speed for anticyclonic vortex flow. This value turns out to be 0.1 m/s for a vortex the size of Conamara Chaos.

[95] However, this upper speed limit is rarely reached by geophysical flows. The ratio of flow speed to the above speed limit, $\epsilon = u/u_{\max}$, is equivalent to the "Rossby number" [*Holton*, 1992]. In large-scale and mesoscale flows in Earth's atmosphere and oceans, ϵ rarely exceeds 10^{-1}, and is generally much smaller [*Gill*, 1982; *Pedlosky*, 1987]. Thus T&D's technique leads to a substantial overestimate of plume current speeds.

[96] Our technique makes use of the thermal wind equation, which balances hydrostatic pressure gradients caused by buoyancy variations against Coriolis effects. While this technique is not perfect, it suggests flow velocities of 3–8 mm/s, which is 1–2 orders of magnitude slower than T&D's estimate.

6. Effect of Plumes on the Ice Layer

6.1. Plume Diameter and Chaos Dimensions

[97] Figure 7 demonstrates that the expected equilibrium size of the central plume (25–50 km) is significantly smaller than the size of the Conamara Chaos (75–100 km), and yet much larger than the vast majority of lenticulae or "micro-chaoses" (<15 km). A comparison of these scales is shown in Figure 10. In the melt-through scenario described by *O'Brien et al.* [2002] [see also *Greenberg et al.*, 1999], the size of the melt-thinned patch always grows rapidly to match the area over which heating is supplied. Since the lenticulae are several times smaller than the pool of warm water produced by a hydrothermal plume, they are probably formed by a different process.

[98] On the other hand, a large hydrothermal plume is the right size to lead to the formation of the entire Conamara Chaos region. As we argued in section 4.3.3, warm eddies will heat the base of the ice out to a distance somewhat larger than l_{cone}, so that the diameter of strong plume heating is comparable to the diameter of the chaos.

[99] One argument against our conclusion that lenticulae/micro-chaoses are too small to be formed by melt-through observes that since heating intensity weakens as one moves away from the axis of the plume, the ice is removed more quickly at the center, and more slowly farther away. Thus the diameter of the melt-through zone increases with time. Perhaps plumes are short-lived, and heat output ceases long before the melt-through diameter exceeds the characteristic width of the plume heating. But such a hypothesis is inconsistent with the observed distribution of micro-chaos/lenticulae. Figures 7 and 8 of *O'Brien et al.* [2002] show that melt-zone diameter increases very rapidly at first, then levels out as time goes on. Thus only a very narrow range of plume lifetime could produce a small melt-through feature. Below a critical lifetime we get no melt-through at all; 20% longer, and the melt-through diameter is close to the diameter of the heat source. Thus the model of *O'Brien et al.* [2002] implies that small areas of chaotic terrain (<20 km diameter) should be rare. This does not agree with the chaos/lenticulae size distributions measured by *Riley et al.* [2000] or *Spaun et al.* [2001]: features <15 km are the

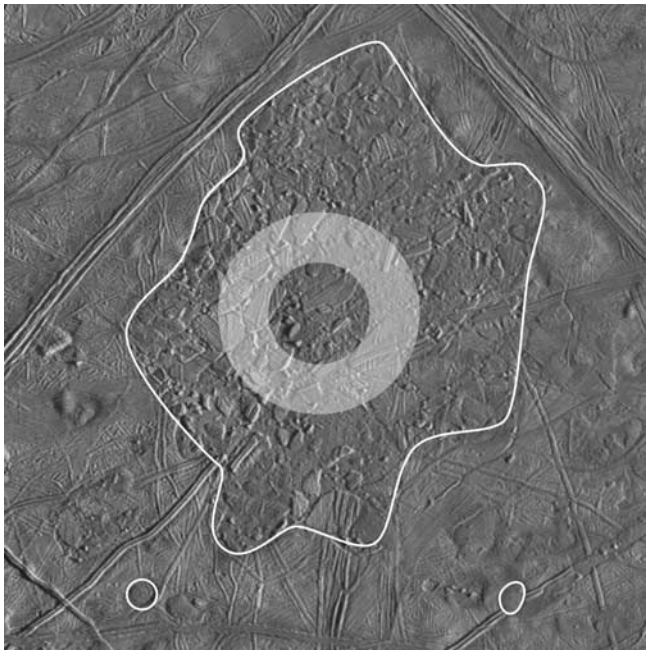

Figure 10. Size comparison of Conamara Chaos and lenticulae with predicted plume diameter l_{cone}. White outlines show approximate boundaries of Conamara Chaos (large irregular outline at center) and of two representative lenticulae (small round outlines at bottom). Shaded circular zone shows range of predicted plume diameters (25–50 km). Base image is from Galileo Orbit E6 imagery.

most abundant. We make this argument more formally in Appendix A.

6.2. Satellite Lenticulae

[100] Noting that lenticulae are often found near large chaos regions, T&D suggest that they might be formed by heat released by baroclinic eddies that spin off the main convective plume. This can only occur if the eddies remain stationary relative to the ice sheet for long enough to achieve significant melting. Calculations by *O'Brien et al.* [2002], T&D, and us (J. C. Goodman et al., An improved melt-through model for chaos formation on Europa, manuscript in preparation, 2004) (hereinafter referred to as Goodman et al., manuscript in preparation, 2004) agree that the melting process takes O(10,000 yr) to occur. Thus, for an eddy to create a lenticula, it must drift no more than one lenticula-diameter in 10,000 years, implying a drift velocity slower than 1 meter per year. As we have demonstrated, eddy drift rates are many orders of magnitude larger than this. Thus freely drifting eddies would move away too quickly to form satellite lenticulae. T&D's other hypothesis, that the lenticulae are formed by smaller hydrothermal vent sources in the vicinity of the main vent site, is problematic because of the diameter comparison argument above.

6.3. Heat Fluxes and Melt-Through

[101] Are the heat fluxes produced by a hydrothermal plume sufficient to melt entirely through the ice layer, and if so, how much time is required to do so?

[102] Thomson and Delaney present a calculation of the time required for a hydrothermal plume to melt through Europa's ice layer. They do this by computing the heat capacity H_{cc} of a slab of ice the size of Conamara Chaos, 2–5 km thick, and then dividing by the heat output of an assumed hydrothermal source:

$$t_{cc} \approx H_{cc}/F_{cc}$$

F_{cc} is computed by dividing an estimate of Europa's global thermal output by the fraction of planetary area occupied by the Chaos. There are several problems here, both in concept and in execution:

[103] • All the basal heat input is assumed to go into melting ice. No heat is permitted to conduct through the ice slab and escape to space. We have built a melt through model (discussed below and in Appendix B) which demonstrates that thermal conduction is a crucial part of this process, and renders complete melt-through impossible for the heat fluxes considered by T&D.

[104] • To compute F_{cc}, T&D assume "uniform partitioning of the global heat flux over the surface of Europa."; that is, they assume the heat flux supplied to the chaos (in W/m^2) is the same as the planetary average value. If the chaos represents the influence of a hot spot, the heat flux should be above average. If melt-through occurs for planetary-average heat fluxes, why is the entire surface not melted? The answer lies in the neglect of thermal conduction, as described above.

[105] • T&D have neglected a factor of 4 in the planetary-surface-area term in their equation (30) for F_{cc}.

[106] Our description of the turbulent mixing of the plume provides a better estimate of the surplus heat flux per unit area applied to the base of the ice layer. The heat fluxes predicted in section 4.3.3 may be used in a simple thermodynamic model of a conducting ice layer to predict the response of the ice layer to these heat fluxes. The model we used is summarized in Appendix B, and described fully by Goodman et al. (manuscript in preparation, 2004, and references therein). This model predicts that, for the range of heat fluxes shown in Figure 8, a substantial thickness of ice remains unmelted. Conduction and radiation carry away enough heat to bring melting to a halt before melt-through occurs. Equilibrium thickness is roughly inversely proportional to heat flux, ranging from 2.5 km for a 0.1 W/m^2 flux to 40 m for a 10 W/m^2 flux. This conclusion differs from that of *O'Brien et al.* [2002]; an explanation for this is given in Appendix B.

[107] Note that the smallest-diameter plumes, those closest to the scale of the abundant lenticulae, have miniscule heat fluxes, which leave unmelted several km of ice. This makes it even harder to explain lenticulae as products of melt-through.

[108] A thin remnant ice layer behaves differently than a liquid lake in several respects; one of the most important is its impact on the drift of ice rafts.

6.4. Ice Raft Drift

[109] T&D argued that the apparent motion of ice blocks in Conamara Chaos could result if the ice rafts were freely drifting in currents produced by a hydrothermal plume. By reassembling the blocks in jigsaw-puzzle fashion, *Spaun et al.* [1998] measured the rafts' motion during chaos forma-

tion, and reported a clockwise sense of revolution of the field of rafts. T&D note that this is consistent with currents generated by a hydrothermal plume system at Conamara's location.

[110] However, Spaun et al. give no error analysis for their drift vectors. Many of the largest drift vectors are badly constrained along the east-west axis; many blocks in the south-central part of the chaos were assumed to have originally been part of a ridge aligned E-W. This fixes their original location perpendicular to the ridge, but their position along the ridge remains uncertain (N. Spaun and G. C. Collins, personal communication, 2002). Thus the evidence for circular motion is rather ambiguous. Also, there is no tendency for individual blocks to rotate clockwise, as rafts freely drifting in a fluid with clockwise vorticity ought to do.

[111] Suppose we take Spaun's drift directions at face value. Could ocean currents push the ice rafts to their new locations in a reasonable amount of time? Assuming the apparent displacement of ice blocks in Conamara Chaos is a result of advection by plume currents, T&D deduced that the ice rafts must have been free to drift for roughly 22 hours in order to drift as far as observed (8 km), assuming current speeds of O(0.1 m/s). Using our revised velocities (3–8 mm/s), we find that 2 weeks to a month are required to move the blocks.

[112] This calculation assumes that the ice blocks are completely free to drift with the current. In contrast, we argue (Goodman et al., manuscript in preparation, 2004, and references therein; see Appendix B) that total melt-through is unlikely; a substantial thickness of frozen material remains surrounding the blocks, impeding their motion.

[113] Let us estimate the drag of ocean currents on a typical ice raft. Suppose, as suggested by *Greenberg et al.* [1999] and T&D, that the ice rafts represent floating ice blocks O(1 km) thick [*Carr et al.*, 1998; *Williams and Greeley*, 1998], broken off from less-melted crust. We suppose that these blocks are embedded in a matrix of solid ice at least O(10 m) thick, a lower limit on the thickness of unmeltable ice computed by the thermodynamic ice model described by *Goodman et al.* (manuscript in preparation, 2004, and references therein), given the heat flux values predicted in section 4.3.3.

[114] We shall assume that the matrix material resembles terrestrial sea ice, recognizing that the matrix is probably stiffer due to its colder temperature. Terrestrial sea ice behaves as a plastic material [*Hibler*, 1979; *Overland et al.*, 1998]; its rate of strain is negligible until a critical stress is exerted. Thus the ice raft cannot drift unless the drag force of the flowing water upon the raft exceeds the yield strength of the surrounding matrix. Otherwise, it remains locked in place. The drag force is

$$F_{\text{drag}} = c_D \rho_w u^2 A_x$$

where c_D is the drag coefficient, a constant of order unity; A_x is the cross-sectional area of the raft, ρ_w is the density of water, and u is the flow velocity. Assuming a cylindrical ice raft 1 km thick and 10 km in diameter, with $u = 5$ mm/s and $c_D \sim 1$, we find that $F_{\text{drag}} \sim 2.5 \cdot 10^5$ N. This force is applied as a stress along the raft-matrix interface. For a matrix thickness of 10 m, this interface has an area of $3 \cdot 10^5$ m^2, resulting in an average stress along the boundary of 0.8 Pa. At various positions around the boundary, this stress may be compressive, tensile, or shear, but the order of magnitude is all that is needed for our purposes.

[115] Numerical models of terrestrial sea ice deformation [*Hibler*, 1979] use a yield strength parameter of O(10^4) Pa for sea ice. More recent modeling studies of the drift of giant icebergs in the ice-covered Weddell Sea [*Lichey and Hellmer*, 2001] find that icebergs are rigidly locked into solid sea ice until stresses exceed a similar value. Cold Europan ice should be even stronger than terrestrial ice.

[116] Thus the drag force caused by ocean currents is many orders of magnitude too weak to permit an ice raft to move through the matrix material. The drag force is so weak that the ice need not be intact to impede raft motion; even slush has enough strength. Observe that the predicted stress ($\sim$1 Pa) is much less than that exerted by the weight of a cocktail umbrella on the slush in a frozen daiquiri.

[117] We conclude that some other force must be responsible for the observed ice motion. The traction of warm, ductile subsurface ice (discussed further in section 8) is one possibility.

6.5. Thermal and Dynamical Stresses

[118] T&D computed the upward pressure exerted by the plume's buoyancy and its momentum. They found that these pressures are small, and would be balanced by surface topographic variations of <1 cm. Our plumes generally have even weaker temperature anomalies, so our values would be even smaller. The direct mechanical effect of the plume's buoyancy on the ice is negligible.

[119] A back-of-the-envelope calculation shows that the thermal stresses which would result from warming the ice during a melting event would exceed its brittle strength. However, since the temperature ramps up over a long time ($\sim 10^4$ y), stress will develop over a period much longer than the Maxwell time so long as the viscosity of the warmed ice is $\ll 10^{20}$ Pa-s (assuming rigidity values quoted by *Moore and Schubert* [2000]). In this case, the thermal expansion can be accommodated by viscous deformation, and no cracking need occur.

6.6. Viscous Deformation

[120] We have argued that melt-through models are unlikely to explain the scales of Europa's small lenticulae, and the motion of ice rafts in Conamara Chaos. Viscous flow of warm, ductile ice beneath the cold, brittle surface is one possible alternative mechanism for chaos formation, which is compatible with hydrothermal plume heating. A small hydrothermal heat source could excite ice diapirism, as described by *Pappalardo et al.* [1998] and *Nimmo and Manga* [2002]. A larger heat source could thin the ice sheet through melting; the resulting isostatic adjustment would create a pressure gradient that could push viscous basal ice toward the thin spot. This flow might drive ice-raft motion. *O'Brien et al.* [2002] demonstrated that this flow was too slow to counteract melt-through of the ice layer, but perhaps it could transport ice rafts laterally a few km, accounting for the motion observed by *Spaun et al.* [1998]. We are

presently investigating this possibility. A preliminary calculation suggests that in some cases, ice inflow velocities may exceed 25 cm/yr at the base of the ice layer.

7. Salinity Considerations

[121] Our discussion thus far has assumed that heating via seafloor hydrothermal activity is the only source of buoyancy in the liquid layer. However, planetary chemical evolution models [*Kargel et al.*, 2000; *Fanale et al.*, 2001] and a possible detection of salts on Europa's surface [*McCord et al.*, 1998] suggest that the ocean is salty. Salt is not readily incorporated into ice as it freezes, so negatively (positively) buoyant fluid is released as ice forms (melts). We must consider this buoyancy source in our analysis.

[122] If Europa's ocean were in a steady-state balance, with uniform heat output everywhere and no net melting or freezing, there would be no saline buoyancy source. But since the salty brine rejected by freezing sinks to the bottom, while the fresh water formed by melting floats at the ice/water interface, a nonuniform (in space or time) heat output would tend to stratify the ocean; this counteracts the tendency of seafloor geothermal heating to remove stratification.

[123] Brine rejection upon freezing represents a negative buoyancy source at the top of the ocean. This is no different from the negative buoyancy formed by cooling as heat is conducted into the ice; it promotes descending turbulently mixing plumes and the removal of stratification. However, melting ice forms a thin layer of fresh water at the ice-water interface. What happens to this layer? Does it lead to a large-scale stratification of the ocean layer?

[124] Since water contracts as it melts, the buoyant fresh liquid formed by melting a localized patch of ice would be trapped in the melted concavity in the ice. This would prevent lateral outflow of the buoyant meltwater, and limit the surface area over which mixing and diffusion can modify the salinity; only vertical exchanges across the horizontal base of the melt pool need to be considered.

[125] Salt would tend to diffuse from the saline water below into the meltwater above. However, heat diffuses 100 times faster than salt. This leads to the phenomenon of "double diffusion" [*Schmitt*, 1994]. In situations like ours, where cold fresh water lies above warm salty water, the "diffusive layering" phenomenon occurs. Suppose the interface is perturbed downward, so that a cold fresh parcel is surrounded by warm salty water. Heat diffuses into the parcel faster than salt, resulting in a net gain of buoyancy. The parcel thus tends to rise upward, returning to the fresh layer. The transfer of heat (with little transfer of salt) from the lower layer to the upper layer adds buoyancy to the base of the upper layer, driving turbulent Rayleigh-Benard mixing. The same happens in the lower layer as its top is cooled. Thus the layers become homogenized, and the layer interface is sharpened. This nonintuitive result (that diffusion can lead to a sharpening of gradients) is well documented in laboratory experiments and observations of Earth's oceans [*Schmitt*, 1994].

[126] Thus buoyant fresh fluid would tend to be confined to a narrow zone directly beneath an area undergoing active melting, with a very sharp interface separating it from the denser, unstratified saline fluid beneath. What impact would this have on the behavior of the buoyant hydrothermal plumes considered in this paper? Plumes would experience unstratified conditions in the lower layer as they form and rise. Their buoyancy anomaly would be less than the buoyancy jump across the double-diffusive layer interface, so they would be unable to penetrate it. Therefore plume fluid must spread outward below the interface; the interface behaves like a solid boundary, impeding the upward motion of the fluid. Heat would be transferred across the interface and into the melt layer via thermal conduction across a thin boundary layer, just as it would be if the plume directly contacted the ice. Thus the length and velocity scales predicted in section 3 remain relevant when salinity changes caused by melting are included.

8. Conclusions

[127] Beginning with the assumption that a $\sim$100 km-thick ocean layer lies beneath Europa's icy crust, we have described the response of the liquid layer to a local seafloor heat source of diameter $\lesssim$5 km.

[128] Hydrothermal plumes constrained by Coriolis forces can supply focused heating to the base of Europa's ice shell. *Thomson and Delaney* [2001] have invoked hydrothermal plumes as agents for the formation of lenticulae and chaos on Europa. Using scaling analysis supplemented by laboratory experiments, we have built up a dynamically consistent picture of the formation and behavior of these plumes.

[129] Over a wide range of plausible ocean thicknesses and plume heat source magnitudes, we predict that equilibrium plume diameters range between 20 and 50 km. This is much larger than the size of Europa's lenticulae; thus the scales of the lenticulae must be set by some other process (see Appendix A for a detailed argument). On the other hand, the size of the plume and its associated warm eddies is consistent with the size of large chaos regions such as Conamara.

[130] The heat flux per unit area supplied by a plume to the base of the ice is not well constrained, ranging between 0.1 and 10 W/m^2. However, fluxes in this range do not cause complete melt-through in our model of a conducting ice layer. A layer of ice between tens of meters and a kilometer thick always remains unmelted. While total melt-through seems unlikely, viscous deformation of the ice layer, driven by plume heating and accompanied by incomplete shell melting, presents an alternative formation mechanism.

[131] Ocean currents induced by the buoyant plume are predicted to be 3–8 mm/s. This flow is too weak to cause the observed drift of ice rafts in the Conamara region; the remaining ice matrix can effectively resist the drag force caused by the flow, causing the rafts to be rigidly locked in place.

[132] The most extreme cases we consider, in which melting proceeds to within tens of meters of the surface, may seem tantamount to melt-through. But we have demonstrated that even a thin ice cover is strong enough to prevent the free drift of ice rafts in the melt-through zone. Also, a thin ice cover will prevent the massive release of water vapor by boiling during a melt-through event, which would have important consequences for the deposition of frost on the rest of Europa's surface. The gulf between

the melt-thinning and melt-through descriptions cannot be ignored.

[133] Hydrothermal plumes may be an effective means of locally heating Europa's ice shell. Despite the huge uncertainties in the parameters governing plume behavior, there are fairly strong fluid-dynamical constraints on the plumes, which lead to important insights about the formation processes of chaos and lenticulae on Europa. Further collaboration between the geomorphology and fluid-dynamics communities is necessary to improve our understanding of the interaction of Europa's liquid and solid components, and Europa provides a unique environment in which to test and extend our understanding of geophysical fluid dynamics.

Appendix A: Size Distribution of Chaos/Lenticulae: Observations and Predictions

[134] In section 4.3.2, we noted that the vast majority of lenticulae/chaos features on Europa are smaller than the plume diameters we predicted. We argued from this size mismatch that these features could not be created by plume melt-through. However, in the melt-through model of *O'Brien et al.* [2002], melt-hole diameter increases with time. Could the many small chaos/lenticulae we see result from plume events which shut off before the maximum melt-through diameter is reached?

[135] Let us use O'Brien's results to predict the size distribution of melt-through events. Using O'Brien's Figures 7 and 8, one can demonstrate that for a given heat source diameter d_0, the area A of ice "melted through" in that model is almost exactly proportional to the total energy E (power · time) delivered by the heat source, minus a constant:

$$E = b \cdot (A + A_0) \tag{A1}$$

For source diameter d_0 = 40 km (closest to our predictions for l_{cone}; a conservative estimate if eddy heat redistribution is considered; see section 4.3.2), the best fit to O'Brien's data has A_0 = 240 km^2; $b = 5.2 \cdot 10^{18}$ J/km^2, with a correlation r value of 0.997, an essentially perfect fit. The fit is equally good for all but the very largest choices for d_0.

[136] Now, let $r_e(E)$ be the normalized rate of melting events as a function of energy. That is, the number of events per year with energies between E and $E + dE$ is:

$$dR = r_e(E)dE$$

(note: units of dR are events/yr; r_e is events/(yr-J)).

[137] Let $r_a(A)$ be the normalized rate of melting events as a function of feature area, so the number of melt-through holes created per year with area between A and $A + dA$ is:

$$dR = r_a(A)dA$$

r_a has units of events/(yr-km^2). Note that:

$$r_a(A) = r_e(E)dE/dA$$

Plugging in from (A1):

$$r_a(A) = b \cdot r_e(b \cdot (A + A_0)) \tag{A2}$$

[138] Note the behavior for small chaoses ($A \ll A_0$): r_a approaches the constant value $r_{a0} = b \cdot r_e(b \cdot A_0)$.

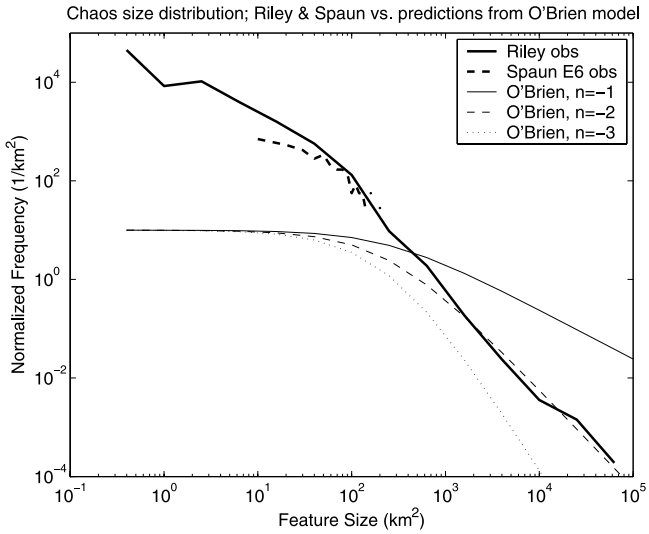

Figure 11. Normalized size distributions for chaos/lenticulae on Europa. Solid thick line: observed distribution from Figure 9b of *Riley et al.* [2000]. For areas between 100 and 10^5 km^2, we use Riley's medium-resolution data; for areas <100 km, we use the high-resolution data. Dashed thick line: same, but for Figure 1 of *Spaun et al.* [2001], E6 orbit data. E11 and E14 data are similar. Thin lines: melt-through size distribution arising from the model of *O'Brien et al.* [2002], assuming a basal heating scale d_0 = 40 km and a power-law distribution of melt-through event energies with various choices of exponent ($n = -1$, $n = -2$, $n = -3$). Y-axis (units 1/km^2) represents number of global features per unit size range, not per unit mapped surface area; thus Riley's data imply 130 features on Europa with sizes between 100 and 101 km^2, 1600 features with sizes between 15 and 16 km^2, etc.

[139] Let n_a be the normalized distribution of chaos/lenticula features on Europa, so the number of chaoses with areas between A and dA is:

$$dN = n_a(A)dA \tag{A3}$$

We will assume that n_a is proportional to the creation rate distribution r_a. This is true so long as there is no preferential destruction of one size class.

[140] *Riley et al.* [2000] and [*Spaun et al.* [1999, 2001] provide size histograms of chaos/lenticulae on Europa. However, Spaun uses a set of equally sized bins, while Riley's bin widths increase geometrically. Since the visual appearance of a histogram can vary radically as one changes the bin sizes, it is very difficult to compare the results of these studies. Thus we normalize the data, dividing the number of features dN in each bin by the width of the bin to generate a normalized frequency distribution n_a (see (A3)). We also divide by the fraction of Europa's surface observed in each study, to produce an estimate of the global population.

[141] These normalized distributions are shown in Figure 11. The dark solid line shows the $n_a(A)$ computed from data in Riley's Figure 9b. Riley's distribution shows power law behavior with an exponent of −2. The thick dashed curve shows n_a for the E6 orbit data from *Spaun et al.* [2001]; their E11 and E14 data are similar, but are

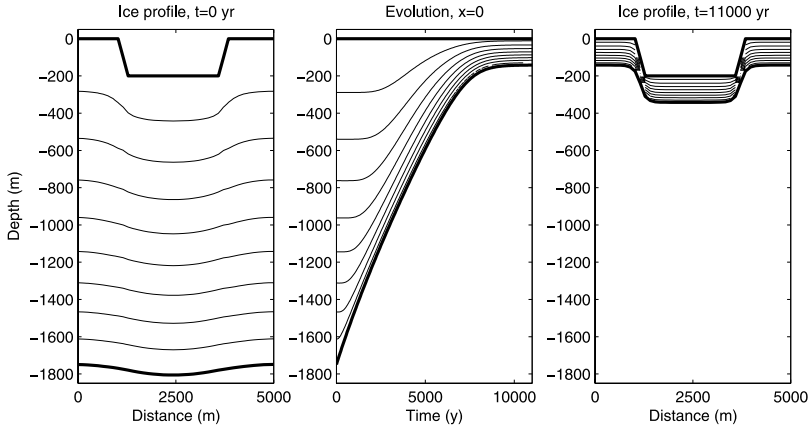

Figure 12. Evolution of 2-D melt-through model, no isostatic adjustment. Left: initial profile. Thick lines show ice boundaries; thin lines show isotherms. Middle: Evolution of ice thickness at $x = 0$ over time, after switching on a 3.3 W/m^2 basal heat source. Ice thins until equilibrium is reached. Right: Equilibrium profile at $t = 11{,}000$ yr. Mean ice thickness is 145 m; minimum is 117 m.

omitted for clarity. Note that when properly normalized, the Riley and Spaun distributions are essentially identical, despite the contrary claim made by *Greenberg et al.* [2003].

[142] Let us now compare these distributions to the predictions that emerge from O'Brien's model. As discussed earlier, (A2) asymptotes to a constant value for small areas. Riley and Spaun's data do not; they increase geometrically down to sizes much smaller than $A_0 = 240$ km^2. Thus the O'Brien formation mechanism is inconsistent with the observed distribution of chaoses, given our predictions for plume diameter.

[143] In Figure 11, we also show plots of r_a (equation (A2)), assuming that the energy distribution $r_e(E)$ of melt-through events, like many other geophysical events, has a power-law distribution. No matter what power exponent we choose, we cannot fit the observed chaos distribution; this remains true for non-power-law distributions. The only way to match the data is to choose a special $r_e(E)$ which has an infinite spike at the energy value $E_0 = b \cdot A_0 = 1.25 \cdot 10^{21}$ J. This is highly unlikely; why would volcanoes on the seafloor regularly vent for precisely the amount of time required to barely melt through the ice shell? One might also match the data by assuming a very narrow-diameter heat source, which would reduce A_0. But the required source diameter ($\ll$20 km) is ruled out by the plume dynamics discussed in the main body of this paper.

Appendix B: Can the Ice Shell be Completely Melted?

[144] In this section, we discuss the "melt-through" process in more detail. We argue that the heat fluxes described in section 4.3.3 are unlikely to melt completely through Europa's ice layer at any location.

[145] *O'Brien et al.* [2002] (OGG hereafter) use a two-dimensional finite-volume model to describe thermal diffusion within the ice layer. The layer is assumed to be initially 6 km thick, and is broken up into cells 100 m in width and thickness. They apply a local heat source of 50–500 GW beneath the ice, over a horizontal extent ranging between 20 and 200 km. This heat melts the ice away cell-by-cell, until a balance is reached between heat input and thermal diffusion, or until the ice disappears entirely. They find that melt-through occurs in O(100) years to O(10,000 years), depending on the intensity of the heat source.

[146] Melting entirely through the ice layer is inconsistent with a simple surface energy balance, given reasonable basal heat inputs. To balance thermal radiative emission from the surface to space against heat input via insolation and subsurface heating requires:

$$F_{\text{base}} = \sigma T^4 - F_{\text{solar}} \tag{B1}$$

With an (open-water) albedo of 0.1, the maximum time-averaged absorbed solar radiation is $F_{\text{solar}} = 14$ W/m^2. The outgoing thermal radiation for a 273-K blackbody is 315 W/m^2. Thus the subsurface heat source must provide $F_{\text{base}} = 300$ W/m^2 to maintain liquid at the surface. This is far less than the heat fluxes (0.01–10 W/m^2) predicted by our work. OGG's standard cases (50 and 500 GW over a 200-km-wide patch) are also too small, providing only a maximum of $F_{\text{base}} = 3.3$ and 32 W/m^2. The balance above does not include latent heat loss by vaporization; this could amount to hundreds of W/m^2 of additional heat loss.

[147] In steady-state balance, then, an ice layer remains. Its thickness can be computed by equating the thermal conduction through the ice layer with the heat source at the base and the heat loss at the surface. We use a one-dimensional vertical diffusive balance, ignoring lateral diffusion, and neglecting latent heat loss from the surface. Ice flow and energy generated by tidal dissipation within the ice shell are also ignored, as OGG demonstrate them to be small.

$$k\frac{\partial}{\partial z}T = F_{\text{base}} = \sigma\left(T|_{z=0}\right)^4 - F_{\text{solar}}$$

$$T|_{z=-h} = T_f \qquad k = b_1/T + b_0$$

where T_f = 273 K, b_1 = 488 W/m, and b_0 = 0.468 W/m/K [*Hobbs*, 1974]. We may solve for surface temperature and ice thickness:

$$T_s \equiv T|_{z=0} = [(F_{\text{base}} + F_{\text{solar}})/\sigma]^{1/4}$$
$$h = \frac{b_1 \log(T_f/T_s) + b_0(T_f - T_s)}{F_{\text{base}}} \quad \text{(B2)}$$

[148] If F_{base} = 3.3 W/m^2 and F_{solar} = 8 W/m^2, T_s = 119 *K*, h = 143 m. If F_{base} = 32 W/m^2, (OGG's higher estimate) T_s = 162 *K*, h = 10 m.

[149] Why, then, do OGG find zero ice thickness in their model? The accuracy of OGG's model is impaired by their numerical scheme. Their domain is broken up into cells 100 m thick; each cell is either entirely water or entirely ice. Thus the model cannot distinguish between, say, 50 meters of ice and zero ice. In addition, as the ice layer becomes only one or two gridpoints thick, the thermal structure within the ice layer becomes unresolved.

[150] We have addressed this issue by constructing a model substantially identical to OGG's, but whose resolution improves as the ice becomes thinner. It consists of 20 vertical levels evenly spaced between the top and bottom of the ice. Full details of this model are described by Goodman et al. (manuscript in preparation, 2004, and references therein). The model also permits irregular surface topography and isostatic adjustment; in all other respects, it is identical to OGG's. The melt-through process is halted in our model by a slight warming of the surface, which allows the surplus basal heat to be lost to space (see (B1)). When run in circumstances identical to OGG's, it evolves to an equilibrium identical to that described by equation (B2). In contrast to OGG's model, at no point during the evolution does open water occur. This is a consequence of our adequate resolution of thin ice layers.

[151] If the surface of the ice prior to melt-through contains hills and valleys larger than the post-melting equilibrium ice thickness, does that mean that open water can be found in the former valleys? No. We illustrate this using our improved melt-through model in Figure 12. We begin with an ice layer 1700 m thick; surface topography includes a flat-bottomed valley 200 m high and 2 km wide. A spatially uniform 3.3 W/m^2 heat source is switched on at t = 0. As equilibration occurs, the basal surface conforms to the surface topography; at no point is the ice thinner than 110 m in this experiment.

[152] Note that the equilibrium profile is not isostatically compensated; if total isostatic adjustment is included, with appropriate changes in initial conditions, the ice equilibrates to a uniform thin layer sans topography, never thinning to less than 140 meters. These two cases (total and zero isostatic adjustment) probably bracket the true behavior of Europa's ice. Similar results to those presented here are obtained for a variety of heating intensities and surface elevation profiles, including mesas and deep crevasses (Goodman et al., manuscript in preparation, 2004, and references therein). As a general rule, when a model with adequate resolution is used, total melt-through does not occur unless basal heat flux reaches hundreds of W/m^2.

[153] **Acknowledgments.** The tank experiments were performed at the GFD lab in the department of Earth, Atmospheric, and Planetary Sciences at MIT, with the assistance of Gordon Brown and Dawn Ash. Richard Thompson provided valuable discussion regarding plume dynamics. We are also grateful to W. Moore and an anonymous reviewer for their very helpful suggestions.

References

Anderson, J. D., G. Schubert, R. A. Jacobson, E. L. Lau, W. B. Moore, and W. L. Sjogren (1998), Europa's differentiated internal structure: Inferences from four Galileo encounters, *Science*, *281*, 2019–2022.

Baker, E. T., and G. J. Massoth (1987), Characteristics of hydrothermal plumes from two vent sites on the Juan de Fuca ridge, northeast Pacific, *Earth Planet. Sci. Lett.*, *94*, 59–73.

Carr, M. H., et al. (1998), Evidence for a subsurface ocean on Europa, *Nature*, *391*, 363–365.

Chyba, C. F., and C. B. Phillips (2002), Europa as an abode of life, *Origins Life Evol. Biosphere*, *32*(1), 47–68.

Collins, G. C., J. W. Head, R. T. Pappalardo, and N. A. Spaun (2000), Evaluation of models for the formation of chaotic terrain on Europa, *J. Geophys. Res.*, *105*(E1), 1709–1716.

Cowling, T. G. (1957), *Magnetohydrodynamics*, *Intersci. Tracts Phys. Astron.*, vol. 4, Wiley-Interscience, New York.

Fanale, F. P., Y.-H. Li, E. De Carlo, C. Farley, S. K. Sharma, and K. Horton (2001), An experimental estimate of Europa's "ocean" composition independent of Galileo orbital remote sensing, *J. Geophys. Res.*, *106*(E7), 14,595–14,600.

Fernando, H. J. S., R. Chen, and B. A. Ayotte (1998), Development of a point plume in the presence of background rotation, *Phys. Fluids*, *10*(9), 2369–2383.

Figueredo, P. H., F. C. Chuang, J. Rathbun, R. L. Kirk, and R. Greeley (2002), Geology and origin of Europa's "Mitten" feature (Murias Chaos), *J. Geophys. Res.*, *107*(E5), 5026, doi:10.1029/2001JE001591.

Gaidos, E. J., K. H. Nealson, and J. L. Kirschvink (1999), Life in ice-covered oceans, *Science*, *284*, 1631–1633.

Gill, A. E. (1982), *Atmosphere—Ocean Dynamics*, Academic, San Diego, Calif.

Greeley, R., C. Chyba, J. W. Head, T. McCord, W. B. McKinnon, and R. T. Pappalardo (2003), Geology of Europa, in *Jupiter: The Planet, Satellites and Magnetosphere*, edited by F. Bagenal et al., chap. 15, Cambridge Univ. Press, New York, in press.

Greenberg, R., G. V. Hoppa, B. R. Tufts, P. Geissler, and J. Riley (1999), Chaos on Europa, *Icarus*, *141*, 263–286.

Greenberg, R., P. Geissler, G. Hoppa, and B. R. Tufts (2002), Tidal-tectonic processes and their implications for the character of Europa's icy crust, *Rev. Geophys.*, *40*(2), 1004, doi:10.1029/2000RG000096.

Greenberg, R., M. A. Leake, G. V. Hoppa, and B. R. Tufts (2003), Pits and uplifts on Europa, *Icarus*, *161*, 102–126.

Head, J. W., and R. T. Pappalardo (1999), Brine mobilization during lithospheric heating on Europa: Implications for formation of chaos terrain, lenticula texture, and color variations, *J. Geophys. Res.*, *104*(E11), 27,143–27,155.

Hebert, D., and B. R. Ruddick (2003), Differential mixing by breaking internal waves, *Geophys. Res. Lett.*, *30*(2), 1042, doi:10.1029/2002GL016250.

Helfrich, K. R., and T. M. Battisti (1991), Experiments on baroclinic vortex shedding from hydrothermal plumes, *J. Geophys. Res.*, *96*, 12,511–12,518.

Hibler, W. D. (1979), Dynamic thermodynamic sea ice model, *J. Phys. Oceanogr.*, *9*(4), 815–846.

Hobbs, P. V. (1974), *Ice Physics*, Clarendon, Oxford, England.

Holton, J. R. (1992), *An Introduction to Dynamic Meteorology*, Academic, San Diego, Calif.

Jones, H., and J. Marshall (1993), Convection with rotation in a neutral ocean: A study of open-ocean deep convection, *J. Phys. Oceanogr.*, *23*, 1009–1039.

Jones, H., and J. Marshall (1997), Restratification after deep convection, *J. Phys. Oceanogr.*, *27*(10), 2276–2287.

Julien, K., S. Legg, J. McWilliams, and J. Werne (1996), Rapidly rotating turbulent Rayleigh-Benard convection, *J. Fluid Mech.*, *322*, 243–273.

Kargel, J. S., J. Z. Kaye, J. W. Head, G. M. Marion, R. Sassen, J. K. Crowley, O. P. Ballesteros, S. A. Grant, and D. L. Hogenboom (2000), Europa's crust and ocean: Origin, composition, and the prospects for life, *Icarus*, *148*(1), 226–265.

Kivelson, M. G., K. K. Khurana, C. T. Russell, M. Volwerk, R. J. Walker, and C. Zimmer (2000), Galileo magnetometer measurements: A stronger case for a subsurface ocean at Europa, *Science*, *289*, 1340–1343.

Klinger, B. A., and J. Marshall (1995), Regimes and scaling laws for rotating deep convection in the ocean, *Dyn. Atmos. Oceans*, *21*(4), 222–256.

Lavelle, J. W. (1999), Buoyancy-driven plumes in rotating, stratified cross flows: Plume dependence on rotation, turbulent mixing, and cross-flow strength, *J. Geophys. Res.*, *102*(C2), 3405–3420.

Lichey, C., and H. H. Hellmer (2001), Modeling giant-iceberg drift under the influence of sea ice in the Weddell Sea, Antarctica, *J. Glaciol.*, *47*(158), 452–460.

List, E. J. (1982), Turbulent jets and plumes, *Annu. Rev. Fluid Mech.*, *14*, 189–212.

Marshall, J., and F. Schott (1999), Open ocean convection: Observations, models and theory, *Rev. Geophys.*, *37*, 1–64.

Maxworthy, T., and S. Narimousa (1994), Unsteady, turbulent convection into a homogeneous, rotating fluid, with oceanographic applications, *J. Phys. Oceanogr.*, *24*, 865–886.

McCord, T. B., et al. (1998), Salts on Europa's surface detected by Galileo's Near Infrared Mapping Spectrometer, *Science*, *280*, 1242–1245.

Melosh, H. J., A. G. Ekholm, A. P. Showman, and R. D. Lorenz (2002), Is Europa's subsurface ocean water warm?, *Lunar Planet. Sci.*, *XXXIII*, abstract 1824.

Moore, W. B., and G. Schubert (2000), The tidal response of Europa, *Icarus*, *147*, 317–319.

Nimmo, F., and M. Manga (2002), Causes, characteristics and consequences of convective diapirism on Europa, *Geophys. Res. Lett.*, *29*(23), 2109, doi:10.1029/2002GL015754.

O'Brien, D. P., P. Geissler, and R. Greenberg (2002), A melt-through model for chaos formation on Europa, *Icarus*, *156*, 152–161.

Overland, J. E., S. L. McNutt, S. Salo, J. Groves, and S. Li (1998), Arctic sea ice as a granular plastic, *J. Geophys. Res.*, *103*, 21,845–21,867.

Pappalardo, R. T., et al. (1998), Geological evidence for solid-state convection in Europa's ice shell, *Nature*, *391*, 365–368.

Pappalardo, R., J. W. Head, and the Galileo Imaging Team (1999a), Europa: Role of the ductile layer, *Lunar Planet. Sci.*, *XXX*, abstract 1967.

Pappalardo, R., et al. (1999b), Does Europa have a subsurface ocean? Evaluation of the geologic evidence, *J. Geophys. Res.*, *104*, 24,015–24,056.

Peale, S. J. (1999), Origin and evolution of the natural satellites, *Annu. Rev. Astron. Astrophys.*, *37*, 533–602.

Pedlosky, J. (1987), *Geophysical Fluid Dynamics*, Springer-Verlag, New York.

Riley, J., G. V. Hoppa, R. Greenberg, B. R. Tufts, and P. Geissler (2000), Distribution of chaotic terrain on Europa, *J. Geophys. Res.*, *105*(E9), 22,599–22,615.

Schmitt, R. W. (1994), Double diffusion in oceanography, *Annu. Rev. Fluid Mech.*, *26*, 255–285.

Schulze-Makuch, D., and L. N. Irwin (2002), Energy cycling and hypothetical organisms in Europa's ocean, *Astrobiology*, *2*(1), 105–121.

Spaun, N. A., J. W. Head, G. C. Collins, L. M. Prockter, and R. T. Pappalardo (1998), Conamara Chaos region, Europa: Reconstruction of mobile polygonal ice blocks, *Geophys. Res. Lett.*, *25*, 4277–4280.

Spaun, N. A., L. M. Prockter, R. T. Pappalardo, J. W. Head, G. C. Collins, A. Antman, and R. Greeley (1999), Spatial distribution of lenticulae and chaos on Europa, *Lunar Planet. Sci.*, *XXX*, abstract 1847.

Spaun, N. A., R. T. Pappalardo, and J. W. Head (2001), Equatorial distribution of chaos and lenticulae on Europa, *Lunar Planet. Sci.*, *XXXII*, abstract 2132.

Spaun, N. A., J. W. Head, and R. T. Pappalardo (2002), The spacing distances of chaos and lenticulae on Europa, *Lunar Planet. Sci.*, *XXXIII*, abstract 1723.

Speer, K. G., and J. Marshall (1995), The growth of convective plumes at seafloor hot springs, *J. Mar. Res.*, *53*, 1025–1057.

Spohn, T., and G. Schubert (2003), Oceans in the icy Galileian satellites of jupiter?, *Icarus*, *161*(2), 456–467.

Thomson, R. E., and J. R. Delaney (2001), Evidence for a weakly stratified Europan ocean sustained by seafloor heat flux, *J. Geophys. Res.*, *106*(E6), 12,335–12,365.

Thomson, R. E., J. R. Delaney, R. E. McDuff, D. R. Janecky, and J. S. McClain (1992), Physical characteristics of the Endeavour Ridge hydrothermal plume during July 1988, *Earth Planet. Sci. Lett.*, *111*, 141–154.

Turner, J. S. (1973), *Buoyancy Effects in Fluids*, Cambridge Univ. Press, New York.

Turner, J. S. (1986), Turbulent entrainment: The development of the entrainment assumption, and its application to geophysical flows, *J. Fluid Mech.*, *173*, 431–471.

Visbeck, M., J. Marshall, and H. Jones (1996), Dynamics of isolated convective regions in the ocean, *J. Phys. Oceanogr.*, *26*(9), 1721–1734.

Whitehead, J. A., J. Marshall, and G. E. Hufford (1996), Localized convection in rotating stratified fluid, *J. Geophys. Res.*, *101*(C11), 25,705–25,721.

Williams, K. K., and R. Greeley (1998), Estimates of ice thickness in the Conamara Chaos region of Europa, *Geophys. Res. Lett.*, *25*(23), 4273–4276.

Zimmer, C., and K. K. Khuruna (2000), Subsurface oceans on Europa and Callisto: Constraints from Galileo magnetometer observations, *Icarus*, *147*, 329–347.

G. C. Collins, Department of Physics and Astronomy, Wheaton College, 26 East Main Street, Norton, MA 02766, USA. (gcollins@wheatonma.edu)

J. C. Goodman, Woods Hole Institute of Oceanography, Mail Stop 21, Woods Hole, MA 02543, USA. (jgoodman@whoi.edu)

J. Marshall, Department of Earth, Atmospheric, and Planetary Sciences, Massachusetts Institute of Technology, Room 54-1524, Cambridge, MA 02139-4307, USA. (marshall@gulf.mit.edu)

R. T. Pierrehumbert, Department of Geophysical Sciences, University of Chicago, 5734 South Ellis Avenue, Chicago, IL 60637, USA. (rtp1@geosci.uchicago.edu)